Published in final edited form as:
J Chem Phys. 2016 February 28; 144(8): 084114. doi:10.1063/1.4942165.

General formulation of vibronic spectroscopy in internal coordinates

Alberto Baiardi[1,a], **Julien Bloino**[2], and **Vincenzo Barone**[1]

[1]Scuola Normale Superiore, piazza dei Cavalieri 7, I-56126 Pisa, Italy

[2]Consiglio Nazionale delle Ricerche, Istituto di Chimica dei Composti OrganoMetallici (ICCOM-CNR), UOS di Pisa, Area della Ricerca CNR, Via G. Moruzzi 1, I-56124 Pisa, Italy

Abstract

Our general platform integrating time-independent and time-dependent evaluations of vibronic effects at the harmonic level for different kinds of absorption and emission one-photon, conventional and chiral spectroscopies has been extended to support various sets of internal coordinates. Thanks to the implementation of analytical first and second derivatives of different internal coordinates with respect to cartesian ones, both vertical and adiabatic models are available, with the inclusion of mode mixing and, possibly, Herzberg-Teller contributions. Furthermore, all supported non-redundant sets of coordinates are built from a fully automatized algorithm using only a primitive redundant set derived from a bond order-based molecular topology. Together with conventional stretching, bending and torsion coordinates, the availability of additional coordinates (including linear and out-of-plane bendings) allows a proper treatment of specific systems, including, for instance, inter-molecular hydrogen bridges.

A number of case studies are analysed, showing that cartesian and internal coordinates are nearly equivalent for semi-rigid systems not experiencing significant geometry distortions between initial and final electronic states. At variance, delocalized (possibly weighted) internal coordinates become much more effective than their cartesian counterparts for flexible systems and/or in the presence of significant geometry distortions accompanying electronic transitions.

I Introduction

Electronic spectroscopy remains one of the most used experimental techniques for the study and the characterization of chemical systems. In fact, combining the more standard techniques, like one-photon absorption (OPA) and one-photon emission (OPE), with more recent non-linear techniques, such as resonance Raman (RR)1 and two-photon absorption (TPA),2,3 an extensive characterization of molecular systems is often possible. Furthermore, thanks to the development of chiroptical electronic spectroscopies, such as electronic circular dichroism (ECD) and circularly polarized luminescence (CPL), chiral systems can be investigated with remarkable accuracy. Analysis and interpretation of the rich information provided by experimental spectra can be greatly aided by quantum mechanical (QM) computations. In this regard, the increasing accuracy of methods based on the density

[a] alberto.baiardi@sns.it.

Europe PMC Funders Author Manuscripts

functional theory (DFT) and its time-dependent extension (TD-DFT)4–6 paves the way to reliable computations even for medium- and large-size flexible systems.

However, electronic spectra are usually reproduced with a single peak per electronic transition, band-broadening effects being taken into account by phenomenological and usually symmetric distribution functions. This oversimplified approach, which fully neglects vibro-electronic (vibronic) effects, does not permit a reliable interpretation of high-resolution electronic spectra, where individual vibronic bands are present, but is also insufficient for low-resolution spectra with an asymmetric bandshape. From a computational point of view, the methods developed for the simulation of vibronic spectra can be divided in two main classes: in the so-called time-independent (TI) approaches,7–9 the spectrum is obtained as a sum of individual vibronic transitions, which are treated independently. On the other hand, in the time-dependent (TD)10–12 formulations, based on the pioneering work of Heller,13,14 the vibronic spectrum is obtained as the Fourier transform of the transition dipole moment autocorrelation function. In our group, a general platform has been recently implemented, which supports both TI15,16 and TD17 approaches at the harmonic level, and includes within a single formulation both OPA and OPE, as well as ECD and CPL spectra.16,18 This framework has been since then further extended to the simulation of RR and RROA spectra.19–21 It is noteworthy that this computational tool has been recently extended by some of us to include non-adiabatic effects within the TD framework,22 based on the formulations presented in ref.11,23–25 However, for the sake of simplicity, the current discussion will be set within the Born-Oppenheimer approximation.

Most of the models used to simulate vibronic spectra, both at the TD and TI levels, are based on the harmonic approximation, and the normal modes of both electronic states are usually expressed in terms of cartesian coordinates. However, even if those approximations are well-suited for semi-rigid systems, they become quite inaccurate to describe large and flexible molecules, where large-amplitude deformations accompany electronic transitions. In order to overcome those limitations, anharmonic vibronic models in cartesian coordinates, based either on perturbative26 or variational27 approaches, have been proposed. However, the computational costs of those models grows quickly with the size of the systems, restricting so far their application, to the best of our knowledge, to small-size molecules. A simpler, but still effective solution is offered by the use of a curvilinear set of internal coordinates within the harmonic approximation.28 For vibrational spectroscopies, where a single reference geometry is of interest, it is possible to prove that the same results are obtained in cartesian and internal coordinates, provided that the harmonic approximation is employed. However, for vibronic spectroscopy, two different structures (i.e. the equilibrium geometries of the electronic states involved in the transition) must be described using a single coordinate system. Since the shift between those geometries is not, in general, infinitesimal, the results depend on the coordinate set used. In practice, the quantity which changes with the coordinate system is the Duschinsky transformation. As already discussed by Reimers,29 the vibronic models developed for the cartesian representation still hold in internal coordinates, provided that the Duschinsky transformation is properly formulated for a general set of curvilinear coordinates.30 Therefore, once this generalization has been performed, the same implementation developed for cartesian coordinates can be used.

Several vibronic models in internal coordinates have been already proposed in the literature,[31–35] with promising results for the simulation of vibronic spectra of small- and medium-size flexible systems. However, most of those models are limited to the simulation of OPA spectra within the TI formulation at the Franck-Condon level. Here, a more general approach will be followed, adapted to the versatility of our framework. In order to cover the many diverse features already built within the platform, the extension to support internal coordinates will be presented sequentially, starting from a general discussion on the simulation of one-photon spectroscopies, including the chiral ones. The treatment of Herzberg-Teller effects, which may be significant in several cases, such as for nearly forbidden electronic transitions, as well as for ECD and CPL spectra, will be also discussed. A complete formulation of vertical models in internal coordinates will be also presented, highlighting the approximations under which internal and cartesian coordinates become equivalent. All these extensions are needed in order to support internal coordinates at the same level of approximation as their cartesian counterparts. Furthermore, the reduced-dimensionality schemes, previously derived for the cartesian case,[36] will be extended to internal coordinates. This subject is particularly appealing since, when internal coordinates are used, mode coupling is significantly lower. As a consequence, the use of internal coordinates paves the route toward hybrid schemes, where different modes are treated at different levels of approximation.

Let us recall that most vibronic models proposed until now employ a non-redundant set of internal coordinates based on chemical intuition. However, this task becomes challenging when targeting larger systems. In order to develop a robust, general, and user-friendly computational procedure, an automatic algorithm to select a non-redundant set of internal coordinates starting from the molecular topology must be developed. Even if this problem has been discussed both for geometry optimization techniques,[37–40] and for vibrational spectroscopy,[41–44] it has been rarely analyzed in the field of vibronic spectroscopy, which involves two different electronic states. In our previous work,[45] we showed that delocalized internal coordinates[46] are more reliable with respect to the widely used Z-matrix internal coordinates, especially for systems with a complex molecular topology. In the present work, delocalized internal coordinates will be compared to other choices of internal coordinates generated automatically from the molecular topology in terms of generality and accuracy.

The work is organized as follows: in section II, the theoretical framework of vibronic spectroscopy in internal coordinates is presented, starting from two different algorithms to generate a non-redundant set of internal coordinates. Then, the extension of the theory of vibronic spectroscopy to support also internal coordinates is described, including vertical models and reduced-dimensionality schemes. After the description of the computational details in section III, section IV presents the applications of the theoretical framework to the study of different vibronic spectra of three medium-size systems: imidazole, 4-pentyl-4’-cyanobiphenyl and (1S)-dehydro-epicamphore.

II Theory

A Vibronic models in cartesian coordinates

Before introducing the theory of internal coordinates, it is useful to describe briefly the general framework we are using for the calculation of vibronic spectra in the cartesian representation.15,16,47 Within this framework, absorption and emission one-photon spectra, employing natural or circulary polarized radiation, can be simulated using a single, general formula:16–18

$$I=\alpha\omega^{\beta}\sum_{m}\sum_{n}\rho_{\gamma}\boldsymbol{d}^{\mathrm{A}}_{mn}\boldsymbol{d}^{\mathrm{B}}_{mn}*\delta\left(\frac{E_n-E_m}{\hbar}-\omega\right) \quad (1)$$

where I is a generic experimental observable, ω is the incident frequency, m and n are the molecular states of the initial and final electronic states with energies E_m and E_n respectively, and $\boldsymbol{d}^{\mathrm{A}}_{mn}$ and $\boldsymbol{d}^{\mathrm{B}}_{mn}$ represent generic transition dipole moments between those 2 states, which can correspond to the electric or magnetic dipole moments, for instance, depending on the spectroscopy of interest. Finally, ρ_{γ} is the Boltzmann population of the initial state. The definition of I, $\boldsymbol{d}^{\mathrm{A}}_{mn}$, $\boldsymbol{d}^{B}_{mn}$, γ, a and β is given in table I. In practice, additional approximations must be introduced to use equation 1. First of all, the Born-Oppenheimer approximation is employed to factorize the molecular wavefunction in a nuclear and an electronic part, and non-adiabatic couplings between different electronic states are neglected. Furthermore, the couplings between vibrational and rotational motions are minimized by employing the Eckart conditions.48 Finally, the vibrational wavefunctions of both electronic states are calculated under the harmonic approximation. In the framework of those assumptions, $\boldsymbol{d}^{\mathrm{X}}_{mn}$ can be expressed in terms of the electronic transition dipole moment $\boldsymbol{d}^{\mathrm{X}}_{e,mn}$, where the indexes m and n are used here to label the electronic states $|\boldsymbol{\phi}_m\rangle$ and $|\boldsymbol{\phi}_n\rangle$. Since no analytical expressions for the electronic transition moments are known, a Taylor series with respect to the mass-weighted cartesian normal coordinates $\mathbf{Q}$ about the equilibrium geometry of one of the electronic states is usually employed,

$$\boldsymbol{d}^{\mathrm{X}}_{e,mn}(\mathbf{Q})=\boldsymbol{d}^{\mathrm{X}}_{e,mn}(\mathbf{Q}_{\mathrm{eq}})+\sum_{i=1}^{N_{\mathrm{vib}}}\left(\frac{\partial\boldsymbol{d}^{\mathrm{X}}_{e,mn}}{\partial Q_i}\right)_{\mathrm{eq}}Q_i+\circ(\mathbf{Q}) \quad (2)$$

where X can be either A or B, and N_{vib} is the total number of normal modes. The expansion is commonly limited to the first two terms in equation 2, with the zeroth-order term corresponding to the Franck-Condon approximation49,50 and the first-order correction to the Herzberg-Teller approximation.51 Finally, the linear transformation proposed by Duschinsky30 is used to relate the cartesian-based normal coordinates of the two electronic states,

$$\overline{\mathbf{Q}}=\mathbf{J}\overline{\overline{\mathbf{Q}}}+\mathbf{K} \quad (3)$$

where $\bar{\mathbf{Q}}$ and $\bar{\bar{\mathbf{Q}}}$ are the normal coordinates of the initial and final states, respectively. In the following, single overbar will refer to a quantity related to the initial state and a double overbar to the final state's. **J** is the Duschinsky matrix and **K** the shift vector. The definition of **J** and **K** depends on the model, which is used for the final state PES. Indeed, due to the limitations of the harmonic approximation, two different representations can be chosen. In the first one, referred to as adiabatic, the PES of the final state is expanded about its own equilibrium position (Adiabatic Hessian, AH), while in the vertical one it is expanded about the equilibrium geometry of the initial state (Vertical Hessian, VH). In both cases, simplified models, where mode-mixing as well as frequency change effects are neglected, can be derived (Adiabatic Shift, AS and Vertical Gradient, VG, respectively).15,16

Two parallel approaches can be followed to compute the spectral band-shape. The form of equation 1 corresponds to the time-independent (TI) approach, in which each transition is calculated from the overlap integrals between the vibrational states of the electronic states. These integrals can be obtained either from analytical or recursive formulas.9,52,53 In this approach, the contribution of a single transition to the band-shape can be known precisely, giving the possibility to assign the bands observed in the spectrum, but the computational cost can become unsustainable since the number of transitions is virtually infinite. This hurdle can be greatly reduced by the help of prescreening methods to select the predominant ones, resulting in fast and reliable simulations.54,55 Alternatively, equation 1 can be rewritten within a time-domain representation, as the Fourier transform of the transition dipole moment autocorrelation function.13 An important feature of this time-dependent (TD) model is that, within the harmonic approximation, the autocorrelation function has an analytical expression,10,17,56–58 and therefore the vibronic spectrum can be obtained performing the Fourier integral numerically. Thanks to the automatic inclusion of all transitions, the TD formalism does not suffer from the main drawbacks of the TI framework. Indeed, it is simpler and more cost-effective to generate fully converged band-shapes, especially in presence of temperature effects by the TD route, while the TI one can provide additional information on the contributions of the transitions to each visible band. The computational tool developed in our group supports both the approaches15–17 at the harmonic level, using cartesian coordinates and with the inclusion of all the effects outlined above. Furthermore, it has been more recently extended to the calculation of resonance Raman (RR)19,20,59 and resonance Raman optical activity (RROA)21 spectra. As a conclusion, let us recall that, under the harmonic approximation, the TI and TD approaches share the same set of input data, which are **J**, **K**, the harmonic frequencies of the two electronic states, together with the transition dipole moment and its derivatives. Therefore, in order to support internal coordinates at the harmonic level, the definition of those quantities for curvilinear coordinates must be derived, and then the same formalism as for the cartesian case can be used. Those definitions will be derived in the following sections, within the framework of adiabatic and vertical vibronic models, after a detailed description of several algorithms which can be used to build a non-redundant set of internal coordinates.

B Selection of the non-redundant internal coordinates

In order to extend the vibronic models presented above to support internal coordinates, the well-known Wilson theory28 can be used. Within this framework, the internal coordinates **s**,

which are in general non-linear functions of the cartesian ones **x**, are expanded as Taylor series in power of **x** as reported below:

$$\mathrm{s}_i = \sum_{j=1}^{3N_{\mathrm{at}}} \left(\frac{\partial \mathrm{s}_i}{\partial \mathrm{x}_j} \right)_{\mathrm{eq}} (\mathrm{x}_j - \mathrm{x}_{j,\mathrm{eq}}) + \frac{1}{2} \sum_{j,k=1}^{3N_{\mathrm{at}}} \left(\frac{\partial^2 \mathrm{s}_i}{\partial \mathrm{x}_j \partial \mathrm{x}_k} \right)_{\mathrm{eq}} (\mathrm{x}_j - \mathrm{x}_{j,\mathrm{eq}}) (\mathrm{x}_k - \mathrm{x}_{k,\mathrm{eq}}) + \circ\left(\mathrm{x}^2\right) \quad (4)$$

The matrix containing the first-order derivatives $(\partial s_i/\partial x_j)_{eq}$ is usually referred to as the Wilson matrix **B**. Furthermore, we will refer to the tensor containing the second-order terms $(\partial^2 s_i/\partial x_j \partial x_k)_{eq}$ as the Wilson matrix **B** first derivative **B**′, where $\mathrm{B}'_{ijk} = (\partial \mathrm{B}_{ij}/\partial \mathrm{x}_k)_{\mathrm{eq}} = (\partial \mathrm{B}_{ik}/\partial \mathrm{x}_j)_{\mathrm{eq}}$. The number of elements of a complete set of internal coordinates is equal to the number of vibrational degrees of freedom of the molecule N_{vib} ($3N_{at} - 5$ for linear molecules, $3N_{at} - 6$ otherwise) and therefore **B** is a rectangular $N_{vib} \times 3N_{at}$ matrix. However, the number of internal coordinates is usually larger than N_{vib}, the **s** set is redundant and a non-redundant subset must be extracted before performing the computation.

Within this work, the so-called primitive internal coordinates (PICs) composed, for a single molecule, by all possible bond lengths, valence and dihedral angles, will be used as the redundant set. In order to define unambiguously PICs, a threshold δ_{ij} must be set and two atoms i and j are connected if and only if $|r_i - r_j| \leq \delta_{ij}$. Once the bond connectivity has been defined, the valence and dihedral angles can be defined unambiguously.

PICs, referred to in the following as **s**, are usually redundant, and therefore a non-redundant subset of them, referred to as **s**′ must be determined. The **s**′ coordinates are usually expressed as linear combinations of **s**:

$$\mathrm{s}_i = \sum_{j=1}^{N_{\mathrm{PIC}}} \mathrm{A}_{ij} \mathrm{s}_{j,\mathrm{PIC}} \quad (5)$$

The definition of the matrix **A** changes with the algorithm used to define the non-redundant coordinates. The first route to build non-redundant internal coordinates is based on the so-called delocalized internal coordinates (DICs), which are becoming the most used coordinates in geometry optimizations.[39,46] The algorithm used to generate the DICs is based on the singular value decomposition (SVD) to determine the range and the null space of **B**. Let us calculate the SVD of **B** as follows,

$$\mathbf{B} = \mathbf{U} \Lambda \mathbf{V}^{\dagger} \quad (6)$$

where **U** and **V** are $N_{PIC} \times N_{PIC}$ and $3N_{at} \times 3N_{at}$ square matrices, respectively, whereas **Λ** is a rectangular diagonal matrix (only the elements Λ_{ii} of **Λ** are different from zero). The number of non-null elements of **Λ** is equal to the rank of **B**, which is, in turn, equal to the number of vibrational degrees of freedom of the molecule for a complete set of internal

coordinates. Furthermore, the columns of **U** corresponding to non-zero diagonal elements of **Λ** span the rank of **B**. As a consequence, DICs are defined as follows:

$$s_{i,\mathrm{DIC}} = \sum_{j=1}^{N_{\mathrm{PIC}}} U'_{ij} s_{j,\mathrm{PIC}} \quad (7)$$

where $\mathbf{U}'$ is a $N_{\mathrm{vib}} \times N_{\mathrm{PIC}}$ matrix containing only the columns of **U** corresponding to non-null singular values. This set of internal coordinates has been introduced by Baker and co-workers46 and is usually referred to as delocalized, since it includes linear combinations of internal coordinates of different types localized on different portions of the molecule. Let us recall that, when applied to geometry optimization algorithms, DICs are nearly equivalent to redundant internal coordinates. In fact, when geometry optimizations are performed using redundant internal coordinates, the pseudo-inverse of the redundant Wilson matrix **B** is calculated by means of SVD for each step of the optimization procedure, and this is equivalent to the calculation of DICs at every step. Conversely, in the simulation of vibronic spectra, DICs are calculated taking the equilibrium geometry of one of the two electronic states as a reference and using the resulting coordinate set to describe also the other electronic state. Since the difference between the two equilibrium geometries is, in general, not infinitesimal, the choice of the reference geometry to calculate DICs is relevant.

Different methods have been proposed to avoid the mixing of coordinates of different types. Amongst them, let us recall the so-called weighted internal coordinates (WICs), introduced by Lindh60, where the Wilson matrix **B** is scaled by a square, $N_{\mathrm{PIC}} \times N_{\mathrm{PIC}}$ matrix **W** before identifying the redundancies by calculating the SVD of **WB**. The final set of non-redundant internal coordinates changes with **W** since PICs associated to elements of **W** of significantly different orders of magnitude are not mixed. Even if in the original formulation of Lindh, **W** is an approximation of the exact energy Hessian of the molecule,61 a simpler but still effective procedure has been proposed more recently by Swart,62 where **W** is a diagonal matrix whose elements are expressed in terms of the bond order ρ_{ij} of the atoms involved in the internal coordinate, which is defined as follows:

$$\rho_{ij} = e^{-[(r_{ij}/C_{ij})-1]} \quad (8)$$

where r_{ij} is the distance between the i-th and the j-th atom and C_{ij} is the sum of their covalent radii. Then, the diagonal elements of **W** are calculated using the following relations:

$$\begin{aligned} w_{\mathrm{bond}} &= \rho_{ij} \\ w_{\mathrm{angle}} &= (\rho_{ij}\rho_{jk})^{1/2} [f + (1-f)\sin\theta_{ijk}] \\ w_{\mathrm{dihed}} &= (\rho_{ij}\rho_{jk}\rho_{kl})^{1/2} [f + (1-f)\sin\theta_{ijk}] [f + (1-f)\sin\theta_{jkl}] \end{aligned} \quad (9)$$

where the first expression given in equation 9 is used for each bond between atoms i and j, the second one is used for each angle between atoms i, j and k, where j is the central atom,

and the third equation is used for each dihedral angle between atoms *i, j, k, l*, where the bond between atoms j and k is the central bond. f is a fixed parameter, which is set to 0.12 in agreement with the original work of Swart.62 For the sake of completeness, let us recall that using WICs, a smooth delocalization of the internal coordinates is obtained. In fact, the mixing between coordinates of different types cannot be minimized by calculating the SVD of **B** separately for different types of coordinates, since this procedure may produce an incorrect number of non redundant internal coordinates, and therefore is ill-suited for a general and robust implementation.44

Let us remark that both DICs and WICs give the correct number of non-redundant internal coordinates, except when separate, non-bonded fragments are present in the system under investigation. However, in this case, for each pair of fragments a bond between the two nearest atoms can be added to overcome this problem.

Let us finally recall that the so-called Z-matrix coordinates are still also widely used, since this set is non-redundant by definition. However, as already pointed out for geometry optimizations,37 and discussed by us more recently in the context of RR spectroscopy,45 Z-matrix coordinates are ill-suited for a general and robust implementation. In fact, in the presence of complex molecular topologies, like fused rings of bicyclic structures, it is not straightforward to define a non-redundant Z-matrix with the correct number of parameters. On the other hand, if standard Z-matrices are used, unreliable results are obtained. As a consequence, Z-matrix coordinates will not be used in the following.

C Special cases: out-of-plane and linear angles

The procedure outlined above to build PICs must be modified in presence of particular molecular arrangements. For example, for planar tricoordinated centers, out-of-plane coordinates can be profitably added to better describe deformations from the planar geometry. This coordinate is defined, as the angle between one of the bonds, and the plane defined by the other two bonds28,63 In our implementation, the number of out-of-plane coordinates which are added, as well as the bond used to define them, changes with the number of terminal atoms bonded to the tricoordinated center based on the following rules:

1. in presence of one terminal atom, a single out-of-plane coordinate is added, defined from the bond involving the terminal atom. When two terminal atoms are present, the out-of-plane coordinate defined by the bond involving the third, non-terminal atom, is added.
2. if no terminal atoms are present, the symmetric linear combinations of the three out-of-plane coordinates is included.
3. if the tricoordinated center is part of a ring, the out-of-plane coordinates defined by the bond, which is not part of the ring, is added. The same procedure is adopted when three terminal centers are present (as, for example, in ammonia)

Let us recall that usually, even if the out-of-plane coordinates are not added, the algorithm used to generate DICs and WICs will produce the correct number of non-redundant coordinates. However, the vibrations involving out-of-plane motions would be described in

terms of linear combinations of valence and dihedral angles, and therefore the coupling between different internal coordinates would be higher.

The procedure outlined above to build a non-redundant set of internal coordinates can be further generalized in order to support also linear chains. Let us consider, for example, the general situation sketched in the left panel of figure 1, where the collinear atoms are identified as A, B and D. Using the procedure outlined above, the angle $\widehat{\mathrm{ABD}}$, as well as all dihedrals R_I–A–B–D and A–B–D–L_i (where i is an integer number ≤ 3) are included in the definition of the PICs. However, as already pointed out,64 the values of **B** and $\mathbf{B}'$ for those coordinates diverge, and therefore the numerical stability of the overall procedure is poor. To overcome this limitation, the A–B–D angle is substituted with two appropriate linear bending coordinates, whose definition can be found, for example, in refs.28,63 Furthermore, the dihedral angles involving the A–B–D chain are removed, and all dihedrals R_I–A–C–L_j are added.

By using this protocol, the Wilson matrix **B** and its derivatives can be safely computed, and the final number of non-redundant internal coordinates is correct. This protocol can be further modified to improve the description of linear angles, where the central atom (B in the left panel of figure 1) is a light atom, as occurs, for instance, in hydrogen bonds. In fact, as will be discussed in the following sections, for those systems an incorrect definition of the internal coordinates involving the linear chain may lead to a large coupling between internal coordinates. For the sake of simplicity, let us consider the situation reported in the right panel of figure 1, where the linear chain involves an hydrogen bond with a water molecule. Even if this case is not fully general, the discussion can be easily extended to other hydrogen-bond patterns, as well as to cases, in which the light atom is different. The main limitation of the definition of PICs outlined above for linear chains lies in the two linear bending coordinates. In fact, the definition of $\mathbf{G} = \mathbf{B}\mathbf{M}^{-1}\mathbf{B}^{T}$, which is involved in the calculation of the normal modes in internal coordinates, changes significantly even for small displacements from the linear arrangement, and this introduces the unwanted couplings. In order to overcome this problem, the molecular topology can be modified by substituting the hydrogen bond with the A-O bond. Then, PICs are built following the strategy outlined above, without including the H_A–A–O bond, as well as the two H_O–O–A–H_A dihedral angles. As a conclusion, it is noteworthy that this procedure can be used also when the linear angle does not involve an hydrogen bond. For example, if a valence angle is linear at the equilibrium geometry of only one electronic state, the linear bending coordinates should not be used, since they are ill-suited for the description of the electronic state, where the linear configuration is not present. On the other hand, by using the second procedure, only standard valence coordinates are introduced.

D Adiabatic models in internal coordinates

The Duschinsky transformation can be generalized to support a curvilinear set of internal coordinates. For the sake of simplicity, here we will focus on adiabatic models, whereas the extension to vertical models will be described in the next paragraph. As discussed in the literature28,44, for a single electronic state the harmonic frequencies do not depend on the coordinate system and the same holds true for normal modes in the approximation of

infinitesimal displacements from the equilibrium position. However, this equivalence may not hold for vibronic spectroscopy, since the normal modes are used to describe, through the Duschinsky transformation, the displacement between the equilibrium geometries of the electronic states involved in the transition. Since this displacement is, in general, not infinitesimal, the expression for **J** and **K** changes with the coordinate system.

In order to express the Duschinsky transformation in terms of internal coordinates, the energy gradient and Hessian, **g** and **H** respectively, must be converted from the cartesian to the curvilinear representation. As already discussed in the literature,43,46,65 both **B** and **B**′ are needed to perform this transformation, which is reported below:

$$\begin{aligned}\mathbf{g}_x &= \mathbf{B}^T \mathbf{g}_s \\ \mathbf{H}_x &= \mathbf{B}^T \mathbf{H}_s \mathbf{B} + \mathbf{g}_s{}^T \mathbf{B}'\end{aligned} \quad (10)$$

where the subscripts x and s refer to quantities related to cartesian or internal coordinates respectively. Particular care must be used when the relations given in equation 10 are inverted, since the Wilson matrix **B** for a non-redundant set of coordinates is rectangular (its shape is $N_{\text{vib}} \times 3N_{\text{at}}$). This problem may be solved by including six (or five for linear systems) rows to **B** associated to coordinates representing overall rotations and translations of the molecule.66 However, a simpler solution is offered by the theory of pseudo-inverse matrices. Since **B** is a full row rank matrix, its right Moore-Penrose pseudoinverse is $\mathbf{B}^+ = \mathbf{B}^T(\mathbf{B}\mathbf{B}^T)^{-1}$. As recently discussed by Brandhorst and coworkers67, $\mathbf{B}^+$ can be used to derive the following expressions for $\mathbf{g}_s$ and $\mathbf{H}_s$:

$$\begin{aligned}\mathbf{g}_s &= (\mathbf{B}^T)^+ \mathbf{g}_x \\ \mathbf{H}_s &= (\mathbf{B}^T)^+ \left[\mathbf{H}_x - \mathbf{g}_s{}^T \mathbf{B}'\right] \mathbf{B}^+\end{aligned} \quad (11)$$

Let us recall that, in order to get rid of contributions due to overall translations and rotations, both $\mathbf{g}_x$ and $\mathbf{H}_x$ must be projected onto the pure vibrational subspace of the molecule. While several procedures have been proposed to build the projection matrix **P** to perform this step, 66,68 a simple relation can be derived in terms of the pseudo-inverse $\mathbf{B}^+$ as $\mathbf{P} = \mathbf{B}^+\mathbf{B}$.67 By using $\mathbf{P}\mathbf{g}_x$ in place of $\mathbf{g}_x$ and $\mathbf{P}\left(\mathbf{H}_x - \mathbf{g}_s^T \mathbf{B}'\right)\mathbf{P}$ in place of $\left[\mathbf{H}_x - \mathbf{g}_s{}^T \mathbf{B}'\right]$, the contribution of translations and rotations vanishes.

Once the Wilson matrix $\mathbf{G} = \mathbf{B}\mathbf{M}^{-1}\mathbf{B}^T$ is built, where **M** is the diagonal matrix of the atomic masses, the internal coordinate normal modes $\mathbf{L}_s$ are defined as the eigenvectors of $\mathbf{G}\mathbf{H}_s$. 28,69 The curvilinear normal modes $\mathbf{L}_s$ satisfy the following generalized orthogonality relation:

$$\mathbf{L}_s^T \mathbf{G}^{-1} \mathbf{L}_s = \mathbf{I} \quad (12)$$

As a consequence, the matrix $\mathbf{L}_s$ is not orthogonal, since **G** is not diagonal. Anyway, the definition of the Duschinsky matrix and shift vector in internal coordinates can be derived following the same strategy as in the cartesian case. Let us start from the definition of the curvilinear normal modes $\bar{\mathbf{Q}}_s$ and $\bar{\bar{\mathbf{Q}}}_s$ reported below:

$$\bar{\mathbf{L}}_s\bar{\mathbf{Q}}_s=\mathrm{s}-\bar{\mathrm{s}}_{\mathrm{eq}} \qquad \bar{\bar{\mathbf{L}}}_s\bar{\bar{\mathbf{Q}}}_s=\mathrm{s}-\bar{\bar{\mathrm{s}}}_{\mathrm{eq}} \quad (13)$$

Using the second relation of equation 13 to express **s** in terms of $\bar{\bar{\mathbf{Q}}}$, and using this relation in the first equation, the following expressions for $\mathbf{J}_s$ and $\mathbf{K}_s$ can be derived:29,34

$$\mathbf{J}_s=\bar{\mathbf{L}}_s^{-1}\bar{\bar{\mathbf{L}}}_s \qquad \mathbf{K}_s=\bar{\mathbf{L}}_s^{-1}(\bar{\bar{\mathrm{s}}}_{\mathrm{eq}}-\bar{\mathrm{s}}_{\mathrm{eq}}) \quad (14)$$

where $\bar{\mathbf{L}}_s$ and $\bar{\bar{\mathbf{L}}}_s$ are the transformation matrices from internal coordinates to curvilinear normal modes for the initial and final states, respectively.

The previous equation permits to highlight the origin of the differences between $\mathbf{J}_s$ and $\mathbf{J}_x$. Since our derivation holds for adiabatic models, $\mathbf{g}_x$ vanishes for both electronic states. Therefore, using equation 11, $\mathbf{J}_s$ can be expressed as follows:

$$\mathbf{J}_s=\bar{\mathbf{L}}_x^{T}\mathrm{M}^{1/2}\bar{\mathbf{B}}^{-1}\bar{\bar{\mathbf{B}}}\mathrm{M}^{-1/2}\bar{\bar{\mathbf{L}}}_x \quad (15)$$

As previously discussed45 $\mathbf{J}_s = \mathbf{J}_x$ only if $\bar{\mathbf{B}}^{-1}\bar{\bar{\mathbf{B}}} = \mathbf{I}$. The reference geometry used to compute the first-order derivatives needed to build **B** is different for the two electronic states. As a consequence, the deviation of the product $\bar{\mathbf{B}}^{-1}\bar{\bar{\mathbf{B}}}$ from the identity matrix increases with the extent of the geometry change. As a consequence, for systems undergoing large-amplitude deformations, $\mathbf{J}_x$ and $\mathbf{J}_s$ may be significantly different.

A similar analysis can be performed for the shift vector **K**. Following the same strategy used above, the following relation can be derived:

$$\mathbf{K}_s=\bar{\mathbf{L}}_x^{T}\mathrm{M}^{1/2}\bar{\mathbf{B}}^{-1}(\bar{\bar{\mathrm{s}}}_{\mathrm{eq}}-\bar{\mathrm{s}}_{\mathrm{eq}}) \quad (16)$$

In this case, the indentity $\mathbf{K}_x = \mathbf{K}_s$ holds when $\bar{\bar{\mathbf{s}}}_{\mathrm{eq}} - \bar{\mathbf{s}}_{\mathrm{eq}} = \bar{\mathbf{B}}(\bar{\bar{\mathbf{x}}}_{\mathrm{eq}} - \bar{\mathbf{x}}_{\mathrm{eq}})$. This relation is valid if the difference $(\bar{\bar{\mathbf{x}}}_{\mathrm{eq}} - \bar{\mathbf{x}}_{\mathrm{eq}})$ is small, but this is not the case for flexible system, where the deformation can be significant.

E Extension to vertical models

In order to derive the Duschinsky transformation for vertical models in internal coordinates, a slightly different procedure must be followed, as for cartesian coordinates.70 In this case, the difference between cartesian and internal coordinates is not caused by the presence of two different equilibrium structures, since the reference geometry is the same for both the

PESs. However, the PES of the final state is expanded about a non-stationary point, and therefore the Wilson **B** matrix derivative (**B**′) is needed to calculate the Hessian matrix in internal coordinates. The presence of **B**′ generates the difference between cartesian and internal coordinates, as already discussed by Truhlar and co-workers in deriving the reaction-path Hamiltonian in internal coordinates.43,65

As a first step, let us express the final state potential energy, referred to as $\overline{\overline{V}}$, as a Taylor series about the equilibrium geometry of the initial state in terms of the curvilinear normal coordinates $\bar{\mathbf{Q}}_s$ of the initial state:

$$\begin{aligned}\overline{\overline{V}}(\overline{\mathbf{Q}}_s)&=\overline{\overline{V}}(\overline{\mathbf{Q}}_{s,\mathrm{eq}})+\left(\frac{\partial\overline{\overline{V}}}{\partial\overline{\mathbf{Q}}_s}\right)_{\mathrm{eq}}\overline{\mathbf{Q}}_s+\tfrac{1}{2}\overline{\mathbf{Q}}_s{}^T\left(\frac{\partial^2\overline{\overline{V}}}{\partial\overline{\mathbf{Q}}_s^2}\right)_{\mathrm{eq}}\overline{\mathbf{Q}}_s\\&=\overline{\overline{V}}(\overline{\mathbf{Q}}_{s,\mathrm{eq}})+\overline{\overline{\mathbf{g}}}(\overline{\mathbf{Q}}_{s,\mathrm{eq}})^T\overline{\mathbf{Q}}_s+\tfrac{1}{2}\overline{\mathbf{Q}}_s{}^T\overline{\overline{\mathbf{H}}}(\overline{\mathbf{Q}}_{s,\mathrm{eq}})\overline{\mathbf{Q}}_s\end{aligned}\qquad(17)$$

where $\overline{\overline{\mathbf{g}}}(\bar{\mathbf{Q}}_{s,\mathrm{eq}})$ and $\overline{\overline{\mathbf{H}}}(\bar{\mathbf{Q}}_{s,\mathrm{eq}})$ are the gradient and Hessian of the final state PES calculated at the equilibrium geometry of the initial state and expressed in terms of the normal modes of the initial state. The energy derivatives with respect to the curvilinear normal modes $\mathbf{Q}_s$ can be then expressed in terms of the internal coordinates **s** by taking advantage of the linear relation between those two sets of coordinates:

$$\overline{\overline{\mathbf{g}}}(\overline{\mathbf{Q}}_{s,\mathrm{eq}})=\overline{\mathbf{L}}_s{}^T\overline{\overline{\mathbf{g}}}_s\qquad\overline{\overline{\mathbf{H}}}(\overline{\mathbf{Q}}_{s,\mathrm{eq}})=\overline{\mathbf{L}}_s{}^T\overline{\overline{\mathbf{H}}}_s\overline{\mathbf{L}}_s\qquad(18)$$

Alternatively, the final-state potential energy can be expressed also as a Taylor series in terms of the final-state normal coordinates $\overline{\overline{\mathbf{Q}}}_s$ about their equilibrium position $\overline{\overline{\mathbf{Q}}}_{s,\mathrm{eq}}$, as reported below:

$$\overline{\overline{V}}\left(\overline{\overline{\mathbf{Q}}}_s\right)=\mathrm{E}_{\mathrm{ad}}+\frac{1}{2}\overline{\overline{\mathbf{Q}}}_s{}^T\overline{\overline{\mathbf{\Omega}}}^2\overline{\overline{\mathbf{Q}}}_s\qquad(19)$$

$\overline{\overline{\Omega}}^2$ is a diagonal matrix, whose diagonal elements are the square roots of the harmonic frequencies. In order to express both Taylor expansions in terms of the same coordinate system, the Duschinsky transformation reported in equation 3 can be inverted to express $\overline{\overline{\mathbf{Q}}}_s$ in terms of $\bar{\mathbf{Q}}_s$ as,

$$\overline{\overline{\mathbf{Q}}}_s=\mathbf{J}_s{}^{-1}\overline{\mathbf{Q}}_s-\mathbf{J}_s{}^{-1}\mathrm{K}_s\qquad(20)$$

By using this relation, equation 19 can be written as follows:

$$\begin{aligned}\overline{\overline{V}}(\overline{\mathbf{Q}}_s)=&\tfrac{1}{2}\overline{\mathbf{Q}}_s{}^T(\mathbf{J}_s{}^{-1})^T\overline{\overline{\mathbf{\Omega}}}^2\mathbf{J}_s{}^{-1}\overline{\mathbf{Q}}_s-\mathbf{K}_s{}^T(\mathbf{J}_s{}^T)^{-1}\overline{\overline{\mathbf{\Omega}}}^2\mathbf{J}_s{}^{-1}\overline{\mathbf{Q}}_s\\&+\tfrac{1}{2}\mathbf{K}_s{}^T(\mathbf{J}_s{}^{-1})^T\overline{\overline{\mathbf{\Omega}}}^2\mathbf{J}_s{}^{-1}\mathbf{K}_s+\mathrm{E}_{\mathrm{ad}}\end{aligned}\qquad(21)$$

Equations 17 and 21 must be equivalent for each value of $\bar{\mathbf{Q}}_S$. As a consequence, the coefficients of the zeroth-, first- and second-order terms in $\bar{\mathbf{Q}}_S$ must be equal. The equivalence between the second-order terms can be used to derive the following expression for the Duschinsky matrix $\mathbf{J}_S$:

$$\overline{\overline{\mathbf{H}}}(\overline{\mathbf{Q}}_{s,\mathrm{eq}}) = \left(\mathbf{J}_s^{-1}\right)^T \overline{\overline{\mathbf{\Omega}}}^2 \mathbf{J}_s^{-1} \quad (22)$$

Thus, the Duschinsky matrix $\mathbf{J}_S$ can be obtained by diagonalizing the Hessian matrix in internal coordinates $\bar{\overline{\mathbf{H}}}(\bar{\mathbf{Q}}_S)$. On the other hand, the equivalence of the first-order terms of equations 17 and 21 can be used to derive the following expression for the shift vector $\mathbf{K}_S$:

$$\begin{aligned} \mathbf{K}_s &= -\overline{\overline{\mathbf{H}}}(\overline{\mathbf{Q}}_{s,\mathrm{eq}})^{-1} \overline{\overline{\mathbf{g}}}(\overline{\mathbf{Q}}_{s,\mathrm{eq}}) = -\overline{\overline{\mathbf{H}}}(\overline{\mathbf{Q}}_{s,\mathrm{eq}})^{-1} \overline{\mathbf{L}}_s^T \overline{\overline{\mathbf{g}}}_s \\ &= -\mathbf{J}_s \overline{\overline{\mathbf{\Omega}}}^{-2} \mathbf{J}_s^T \overline{\mathbf{L}}_s^T \overline{\overline{\mathbf{g}}}_s \end{aligned} \quad (23)$$

Following the same strategy as in the previous section, it is possible to prove that equation 23 holds also in the reduced-dimensionality approximation, where $\bar{\mathbf{L}}_\mathbf{s}$ is a rectangular matrix. As a conclusion, let us recall that the previous expressions can be simplified within the VG model, where the Duschinsky matrix is assumed to be equal to the identity matrix **I**. In this case, equation 23 can be recast as,

$$\mathbf{K}_s = -\overline{\overline{\mathbf{\Omega}}}^{-2} \overline{\mathbf{L}}_s^T \overline{\overline{\mathbf{g}}}_s \quad (24)$$

As discussed in ref.45, starting from equation 24 it is possible to prove that the VG model is equivalent in cartesian and internal coordinates. This is the explanation of the better accuracy of vertical models with respect to adiabatic ones in cartesian coordinates when large amplitude deformations are present.34,35,71 However, the equivalence does not hold anymore for the VH model. In fact, as shown in equation 22, the Duschinsky matrix is obtained by diagonalizing the Hessian matrix in internal coordinates $\mathbf{H}_S$, and both the gradient and the Hessian in cartesian coordinates are required to compute $\mathbf{H}_S$. As a consequence, the normal modes obtained issuing from the two representations are not equivalent.

F Reduced-dimensionality schemes

In order to make the computational protocol described above feasible also for large-size systems, we will describe how it can be modified to support also reduced-dimensionality schemes, following the procedure already used for the cartesian case.36 When reduced-dimensionality models are built, a subset of n_{RD} normal modes of one of the states is selected. Those so-called active modes are then used to define a consistent model system, sufficiently uncoupled from the rest of the real system. Vibronic calculations are then carried out on the reduced system. To illustrate the construction of the active ensemble, let us consider as a starting point a subset $\bar{\mathrm{S}}$ of n_{RD} normal modes chosen from the initial state.

The extent of coupling tolerated in the construction of the active block is defined through a positive parameter η, whose value cannot exceed 1. A high value for η ensures that this coupling will be very small. A corresponding subset $\bar{\bar{S}}$ of the modes of the final state can be found such that:

$$\sum_{i\in\bar{S}} J_{ij}^2 \geq \eta \qquad \sum_{j\in\bar{\bar{S}}} J_{ij}^2 \geq \eta \tag{25}$$

The construction of $\bar{S}$ and $\bar{\bar{S}}$ is done iteratively, until their content is stabilized. The number of modes included in $\bar{\bar{S}}$ changes with η. If mode-mixing effects are negligible for the modes in $\bar{S}$, the elements of $\bar{\bar{S}}$ are n_{RD} even for values of η close to 1, otherwise smaller values of η can be used. In this case, a potentially significant portion of **J** may be neglected, lowering the reliability of the reduced-dimensionality approximation. The detailed construction of the model system can be found in refs.8,36

Some care must be paid when this framework must be generalized to internal coordinates. In fact, the relation given in equation 25 assumes that **J** is orthogonal. Indeed, in this case the sums of the squared elements of a row or a column of **J** are equal to 1, and therefore η needs not exceed 1. In order to extend this definition to support curvilinear internal coordinates as well, equation 25 must be modified as follows:

$$\frac{\sum_{i\in\bar{S}} J_{ij}^2}{\sum_{i=1}^{N_{vib}} J_{ij}^2} > \eta \qquad \frac{\sum_{j\in\bar{\bar{S}}} J_{ij}^2}{\sum_{j=1}^{N_{vib}} J_{ij}^2} > \eta \tag{26}$$

The normalization factor of equation 26 sets the upper limit of the sums to 1, and therefore the same definition of η as in the cartesian case can be used.

Once the active normal modes have been selected, the Duschinsky transformation for the reduced-dimensionality scheme must be defined. For curvilinear sets of coordinates, this definition is not as straightforward as in the cartesian case. Let us start from the definition of the curvilinear normal modes given in equation 13 where, for reduced-dimensionality schemes, $\bar{\mathbf{L}}_s$ and $\bar{\bar{\mathbf{L}}}_s$ are $n_{RD} \times 3N_{at}$ rectangular matrices. Following the same strategy used above, the following relation can be derived:

$$\bar{\mathbf{L}}_s \bar{\mathbf{Q}}_s = \bar{\bar{\mathbf{L}}}_s \bar{\bar{\mathbf{Q}}}_s + \bar{\bar{s}}_{eq} - \bar{s}_{eq} \tag{27}$$

Particular care must be used when equation 27 is inverted, since $\bar{\mathbf{L}}_s$ is rectangular. However, equation 12 still holds also for $\bar{\mathbf{L}}_s$ and $\bar{\bar{\mathbf{L}}}_s$, and therefore equation 27 can be inverted by multiplying both lhs and rhs by $\bar{\mathbf{L}}_s^T \bar{\mathbf{G}}^{-1}$. The final definition of $\mathbf{J}_s$ and $\mathbf{K}_s$ is,

$$\mathbf{J}_s = \bar{\mathbf{L}}_s^T \bar{\mathbf{G}}^{-1} \bar{\bar{\mathbf{L}}}_s \qquad K_s = \bar{\mathbf{L}}_s^T \bar{\mathbf{G}}^{-1} (\bar{\bar{s}}_{eq} - s_{eq}) \tag{28}$$

Let us remark that the relations given in equation 28 are equivalent to those, which have been derived by Reimers29 and used more recently by Santoro and coworkers.34 Even if when the full system is considered instead of the reduced-dimensionality one, the relations given in equations 14 and 28 are equivalent, the latter is more general, since it can be extended also to reduced-dimensionality schemes.

G Inclusion of Herzberg-Teller effects

As remarked above, most vibronic models in internal coordinates have been limited to the Franck-Condon approximation,32,34,35,71 and the extension to Herzberg-Teller (HT) effects has been rarely discussed. However, the Franck-Condon approximation can be ill-suited in several cases, such as weakly-allowed or dipole-forbidden electronic transitions, or for chiral electronic spectroscopies (ECD and CPL), where the electric and magnetic transition dipole moments can be nearly orthogonal. Therefore, the inclusion of first-order terms in the transition dipole moment expansion is critical to get a proper simulation of vibronic spectra. With respect to the general discussion at the beginning of this section, a slightly different notation will be adopted here for the sake of readability. The transition dipole moment between the initial (I) and final (F) electronic states will be written as $\boldsymbol{d}^{X}_{IF}$.

First of all, the derivatives of the transition dipole moment must be expressed in terms of the non-redundant internal coordinates $\mathbf{s}'$, starting from the cartesian derivatives. Following the same strategy used to express the energy gradient in terms of internal coordinates, it turns out that only the non redundant Wilson matrix **B** is needed to perform this transformation, which is given as,

$$\frac{\partial \boldsymbol{d}^{\mathrm{X}}_{IF}}{\partial \mathrm{x}} = \mathbf{B}^{T} \frac{\partial \boldsymbol{d}^{\mathrm{X}}_{IF}}{\partial \mathrm{s}} \quad (29)$$

However, **B** must be inverted to use equation 29 in order to express $\left(\partial \boldsymbol{d}^{\mathrm{x}}_{IF}/\partial \mathrm{s}\right)$ in terms of $\left(\partial \boldsymbol{d}^{\mathrm{x}}_{IF}/\partial \mathrm{x}\right)$. Following the procedure used in the previous section, this transformation can be safely performed by using the pseudo-inverse $(\mathbf{B}^{T})^{+}$ and the projector operator **P**,

$$\frac{\partial \boldsymbol{d}^{\mathrm{X}}_{IF}}{\partial \mathbf{s}} = (\mathbf{B}^{T})^{+} \mathbf{P} \frac{\partial \boldsymbol{d}^{\mathrm{X}}_{IF}}{\partial \mathbf{x}} \quad (30)$$

Once the transformation reported above has been performed, the derivative of the transition dipole moment must be expressed in terms of curvilinear normal-modes. The transformation between non-redundant internal coordinates $\mathbf{s}'$ and curvilinear normal modes $\mathbf{Q_s}$ is linear, and therefore $\mathbf{L_s}$ is sufficient to perform this second conversion,

$$\frac{\partial \boldsymbol{d}^{\mathrm{X}}_{IF}}{\partial \mathbf{Q}_{\mathrm{s}}} = \mathbf{L}_{s}{}^{T} \frac{\partial \boldsymbol{d}^{\mathrm{X}}_{IF}}{\partial \mathbf{s}'} = \mathbf{L}_{s}{}^{T} (\mathbf{B}^{T})^{+} \mathbf{P} \frac{\partial \boldsymbol{d}^{\mathrm{X}}_{IF}}{\partial \mathbf{x}} \quad (31)$$

Let us remark that, even if no overbars are specified in equation 31, both **B** and $\mathbf{L}(\mathbf{Q}_s)$ must be calculated with respect to the same reference geometry, which can be either the initial- or the final-state equilibrium geometry, depending on the vibronic model which is used. Even if, for adiabatic models, the previous relation can be further simplified using the same strategy as for equation 15, equation 31 will be preferred in order to make the theoretical derivation as much general as possible.

The coordinates used to express the derivatives of the transition dipole moment depend on the nature of the transition, even if they are usually computed with respect to the excited-state coordinates. For example, in emission spectroscopies (OPE and CPL), those derivatives are usually computed with respect to the final electronic state (which corresponds to the ground state), and therefore an additional transformation is needed. As has been already remarked17,72, the Duschinsky transformation can be used to perform this transformation. However, this framework assumes the orthogonality of the Duschinsky transformation, and must be modified to support also internal coordinates.

To do so, we will derive both the general transformation of the transition dipole moment derivatives from $\bar{\mathbf{Q}}_s$ to $\bar{\bar{\mathbf{Q}}}_s$ and the inverse transformation, from $\bar{\bar{\mathbf{Q}}}_s$ to $\bar{\mathbf{Q}}_s$. By assuming that the HT approximation is exact, the following relation holds:

$$\boldsymbol{d}_{IF}^{X}(\overline{\mathbf{Q}}_{s,\mathrm{eq}})+\sum_{k=1}^{N_{\mathrm{vib}}}\left(\frac{\partial \boldsymbol{d}_{IF}^{X}}{\partial \overline{\mathrm{Q}}_{s,k}}\right)_{\mathrm{eq}}\overline{\mathrm{Q}}_{s,k}=\boldsymbol{d}_{IF}^{X}\left(\overline{\overline{\mathbf{Q}}}_{s,\mathrm{eq}}\right)+\sum_{k=1}^{N_{\mathrm{vib}}}\left(\frac{\partial \boldsymbol{d}_{IF}^{X}}{\partial \overline{\overline{\mathrm{Q}}}_{s,k}}\right)_{\mathrm{eq}}\overline{\overline{\mathrm{Q}}}_{s,k} \tag{32}$$

The Duschinsky relation in internal coordinates, given in equation 14, can then be used to express $\bar{\bar{\mathbf{Q}}}_s$ in terms of $\bar{\mathbf{Q}}_s$. Let us consider the transformation from $\bar{\mathbf{Q}}_s$ to $\bar{\bar{\mathbf{Q}}}_s$. In this case, equation 3 can be used directly to express equation 32 in terms of the coordinates of the final state. Then, the equivalence of the zeroth- and first-order terms of the expansions in the lhs and rhs of equation 32 can be used to derive the following relations:

$$\begin{aligned}\boldsymbol{d}_{IF}^{X}\left(\overline{\overline{\mathbf{Q}}}_{s,\mathrm{eq}}\right)&=\boldsymbol{d}_{IF}^{X}(\overline{\mathbf{Q}}_{s,\mathrm{eq}})+\sum_{k=1}^{N_{\mathrm{vib}}}\left(\frac{\partial \boldsymbol{d}_{IF}^{X}}{\partial \overline{\overline{\mathrm{Q}}}_{s,k}}\right)_{\mathrm{eq}}\mathrm{K}_k\\ \left(\frac{\partial \boldsymbol{d}_{IF}^{X}}{\partial \overline{\overline{\mathrm{Q}}}_{s,k}}\right)_{\mathrm{eq}}&=\sum_{j=1}^{N_{\mathrm{vib}}}\mathrm{J}_{s,kj}\left(\frac{\partial \boldsymbol{d}_{IF}^{X}}{\partial \overline{\overline{\mathrm{Q}}}_{s,j}}\right)_{\mathrm{eq}}\end{aligned} \tag{33}$$

On the other hand, if the derivatives expressed in terms of the coordinates $\bar{\bar{\mathbf{Q}}}\mathbf{s}$ must be expressed in terms of the normal coordinates of the initial state, equation 20 must be used in order to arrive at the following final expression:

$$\boldsymbol{d}_{IF}^{X}(\overline{\mathbf{Q}}_{s,\mathrm{eq}})=\boldsymbol{d}_{IF}^{X}\left(\overline{\overline{\mathbf{Q}}}_{s,\mathrm{eq}}\right)-\sum_{k=1}^{N_{\mathrm{vib}}}\left(\frac{\partial \boldsymbol{d}_{IF}^{X}}{\partial \overline{\overline{\mathrm{Q}}}_{s,k}}\right)_{\mathrm{eq}}\left(\mathbf{J}_{s}^{-1}\mathbf{K}_{s}\right)_{k}$$

$$\left(\frac{\partial \boldsymbol{d}_{IF}^{X}}{\partial \overline{\overline{\mathrm{Q}}}_{s,k}}\right)_{\mathrm{eq}}=\sum_{j=1}^{N_{\mathrm{vib}}}\mathrm{J}_{s,kj}^{-1}\left(\frac{\partial \boldsymbol{d}_{IF}^{X}}{\partial \overline{\overline{\mathrm{Q}}}_{s,j}}\right)_{\mathrm{eq}} \quad (34)$$

III Computational Details

All the computations have been performed with a development version of the GAUSSIAN suite of quantum chemical programs73 extended to the internal coordinate framework presented in section II. Electronic structure calculations were carried out using density functional theory (DFT) and its time-dependent extension (TD-DFT), for ground and excited states, respectively. The B3LYP exchange-correlation functional,74 has been employed in conjunction with the SNSD basis set75, which is obtained adding to the 6-31G(d,p) basis set a minimal number of core-valence (one s function on all non-hydrogen atoms) and diffuse (s,p,d on non-hydrogen atoms and p on hydrogen atoms) functions optimized specifically for global hybrid functionals.76,77

Bulk solvent effects have been included in the QM calculations by means of the polarizable continuum model (PCM),78,79 within its integral-equation formulation (IEF-PCM)80. The solute cavity has been built by using a set of interlocking spheres centered on the atoms with the following radii (in Å): 1.443 for hydrogen, 1.926 for carbon, 1.750 for oxygen and 1.830 for nitrogen, each scaled by a factor of 1.1. The values of the solvent static and dynamic dielectric constants used are $\epsilon = 78.36$ and $\epsilon_\infty = 1.78$ for water, $\epsilon = 24.85$ and $\epsilon_\infty = 1.852$ for ethanol, $\epsilon = 1.911$ and $\epsilon_\infty = 1.925$ for n-heptane. For the sake of uniformity, the equilibrium solvation regime has been enforced in all calculations. A more detailed discussion about different solvation regimes in connection with spectroscopic parameters can be found, for instance, in ref.20

In all TD calculations, the Fourier transform of the transition dipole moment has been computed numerically using a fast Fourier transform (FFT) algorithm, by sampling the autocorrelation function in 224 time steps, for a total time of propagation of 10^{-10} s. Following the computational procedure presented in our previous work,17 a square window function with a width of 216 steps has been used to improve the stability of the numerical integration. For the TI calculations, if not otherwise specified, the standard parameters of the class-based prescreening scheme have been used, which are reported in the following:

$$C_1^{\max}=20, \quad C_2^{\max}=13, \quad N_I^{\max}=10^8$$

where $N_I^{\max}$ is the maximum number of Franck-Condon integrals to compute in a given class, and $C_1^{\max}$ and $C_2^{\max}$ are the maximum excitations of the vibrational levels included in class 1 (overtones) and 2 (combination of 2 modes), respectively. Additional details about the prescreening scheme can be found in refs.54,55 Furthermore, vibrational levels of the

excited states with up to 7 simultaneously exited modes have been taken into account (class 7). In all cases, temperature effects have been neglected.

Regarding the generation of internal coordinates, as outlined in section II, the only input data needed to build the non-redundant internal coordinate set is the molecular topology. In all cases considered in the following, the topology has been generated automatically by the code, defining two atoms X and Y as bonded if their distance is shorter than 130 % of their average XY bond length. Following the GAUSSIAN standard parameters, those values are taken from B3LYP/6-31G(d) results. The well-known analytical expressions for bond lengths, valence, out-of-plane and dihedral angles (given for example in ref.28,64) have been used to generate the redundant Wilson matrix **B**. The analytical expression for the elements of the Wilson matrix **B** and its derivatives for linear bendings is reported, for example, in ref. 63. Finally, in all cases, a threshold of 10^{-5} on the absolute value of the eigenvalues has been used to select the eigenvectors corresponding to non-zero eigenvalues.

IV Examples of Application

A OPA spectrum of imidazole in water

The first test-case is imidazole. Imidazole derivatives are interesting model systems for the more complex biological models, like histidine, as their spectroscopic properties can provide some insights on the latter's. Therefore, several studies, both experimental and theoretical, are available for those systems.81–83 In our recent work,45 the internal coordinate framework presented in section II had been used to simulate the RR spectrum of imidazole using different coordinate systems with the inclusion of solvent effects. In that work we showed that, when solvent effects are included by means of PCM, a large-amplitude deformation of the ring from the planar configuration occurs upon the electronic excitation to the first bright excited state ($\pi \rightarrow \pi^*$ transition), and therefore only by using delocalized internal coordinates can a satisfactory match be reached with the experimental data. On the other hand, using either Z-matrix internal coordinates or the cartesian ones, inaccurate results are obtained. Here, the analysis will be extended to OPA spectroscopy, again with the inclusion of bulk solvent effects by means of PCM. Furthermore, specific solvent effects will be also included by adding two explicit water molecules in the quantum mechanical (QM) simulation, as shown in figure 2, in order to analyse the reliability of our approach in presence of hydrogen bonds.

The comparison of the computed OPA spectra for the $\pi \rightarrow \pi^*$ transition in vacuum using cartesian coordinates, DICs and WICs within both TD (solid lines) and TI (dashed lines) approaches is reported in supplemental figure S1.84 It is noteworthy that the bandshapes obtained using the three different coordinate systems are very close. In fact, the shift between the equilibrium geometries of the ground and excited state is negligible, and all the coordinate systems are equivalent for small geometry deformations. Furthermore, within the same coordinate system, TI and TD results are nearly superimposable. In fact, the convergence of the TI simulation is almost complete (> 99 %), since the Duschinsky matrix is nearly diagonal and the geometry shift is small, so the two methods are expected to give the same results.

In figure 3, the theoretical OPA spectra of imidazole in water computed at the TD AH/FC level using different coordinate systems are reported. Solvent effects have been included by means of PCM, as described in the computational details. At variance with the calculations in vacuum, in this case the overall broadening of the cartesian spectrum is larger than the one of the DIC and WIC spectra, even if the same half-width at half-maximum (HWHM) has been used for each vibronic peak. As remarked before, in this case, even if the five-membered ring is planar in S_0, a significant out-of-plane deformation occurs in the equilibrium geometry of the S_2 excited state. Those deformations are described in an inaccurate way using cartesian coordinates and, as a consequence, a poor definition of the Duschinsky matrix **J** is obtained. On the other hand, DICs and WICs provide nearly equivalent results.

As already pointed out in our previous work,45 the inaccurate description of large-amplitude motions in terms of cartesian coordinates introduces large off-diagonal terms in **J**, which are not present in internal coordinates. The nearly block-diagonal structure of the Duschinsky matrix in internal coordinates opens the possibility of treating normal modes belonging to different blocks at different levels of approximation. For instance, anharmonic models may be used for a limited number of low-frequency modes, whereas the harmonic approximation is used for the other vibrations. The development of such anharmonic models goes beyond the goals of the present work, so that here we will only verify the block-diagonal structure of **J** in delocalized internal coordinates. In this case the five lowest energy normal modes are strongly mixed, but their coupling with the other vibrations is negligible, and may be neglected. In figure 4, the TD AH|FC spectrum obtained neglecting the coupling elements of **J** between those modes and the other ones is reported, together with the spectrum obtained using the full expression of **J**. The two spectra are nearly superimposable, and this result is a confirmation of the block structure of **J**.

The OPA spectrum of imidazole has been simulated also using vertical models. The theoretical spectra calculated at the TD VH/FC level using cartesian and delocalized internal coordinates are reported in figure S2.84 At the equilibrium geometry of S_0, the PES of the S_2 electronic state exhibits two normal modes with imaginary frequencies, which cannot be described at the harmonic level. As a first approximation, those normal modes have been neglected, by uncoupling them from the other ones using the reduced-dimensionality scheme presented in section II. In the cartesian case, η must be set to 0.4, whereas in internal coordinates it can be set to 0.7, and this suggests that the offending modes are more mixed in the cartesian representation than in the internal ones. Even if the theoretical spectra obtained using the different coordinate systems are nearly equivalent (only slight differences can be detected in the spectrum, where a brodadening function with an HWHM of 100 cm^{-1} is used), the definition of the Duschinsky transformation changes significantly. As shown in the graphical representation reported in figure S3,84 the couplings between the two normal modes associated to negative frequencies and the other ones is larger in the cartesian case than in the internal one. For example, the mode $\overline{\overline{1}}$ (ring deformation) of the final state is mostly coupled to the mode $\overline{\overline{2}}$ (ring deformation) of the initial one in internal coordinates, whereas it is significantly coupled to the four modes $\overline{\overline{1}}$-$\overline{\overline{4}}$ in the cartesian representation. As for the low-frequency modes discussed before, imaginary-frequency modes in internal

coordinates are less coupled to the rest of the system, paving the route toward a more accurate treatment for them using low-dimensional anharmonic models.

Specific solvent effects have been simulated including two explicit water molecules in the QM calculation (the structure of the imidazole-water cluster is shown in figure 2), and the results are reported in figure 5. First of all, also for this case, the spectrum in cartesian coordinates is much more broadened with respect to the ones in internal coordinates. Moreover, for the simulations performed using delocalized internal coordinates (green lines), both the standard algorithm used to generate the molecular topology (dashed line), and the one, developed to support the presence of hydrogen bonds (solid line), have been used. Even if the results obtained with the two different algorithms are nearly equivalent, the definition of the Duschinsky transformation changes significantly. The most significant changes are visible in the Sharp and Rosenstock **C** matrix,7,52,54 Within the recursive formulation proposed by Ruhoff, the FC integrals between two vibronic states can be related to lower quanta ones though those matrices. Since temperature effects are neglected here, only final states have excited modes. In this case, as shown in the appendix, the influence of the coupling between the final state modes on the FC integrals is directly related to **C**. The **C** matrix calculated using cartesian coordinates, DICs with the standard connectivity and DICs with modified connectivity in the presence of H bonds are reported in figure 6. First of all, it is noteworthy that the number of off-diagonal couplings between the modes is larger in the cartesian representation than in the internal coordinate case. Furthermore, using DICs, the structure of **C** changes with the used topology. More in detail, even if for the high-energy modes the elements of **C** are nearly equivalent, for the lowest frequency modes, involving a distortion of the hydrogen bonds, the couplings with the other modes are significantly smaller when the modified topology is used. This example shows that, in the presence of weak bonds, such as hydrogen bonds, a careful choice of the coordinate system is critical to describe correctly the normal modes and especially to limit their coupling, even if those differences have a negligible impact on the final vibronic spectrum.

B OPE spectrum of cyanobiphenyl

The second system studied in this work is 4-pentyl-4’-cyanobiphenyl (referred to as 4,4’-CB in the following, and whose structure is reported in figure 2). The central part of this molecule is composed by two bridged phenyl rings, and the PES along the dihedral angle between those rings is usually flat and, upon electronic excitation, the equilibrium value of this dihedral angle may change significantly. This deformation corresponds to a large amplitude motion, and therefore the impact of the coordinate system used in the simulations is expected to be important. It is noteworthy that, unlike simpler biphenyl derivatives, 4,4’-CB contains also a linear CN group, and therefore, by studying this system, it is possible to check the reliability of our implementation in presence of linear structures.

The spectra calculated at the TD AH|FC level using cartesian coordinates, DICs and WICs are reported in the upper panel of figure 7. Like for imidazole, the results obtained using DICs and WICs are nearly equivalent, even if in the low-energy region the WIC spectrum is more intense than the DIC one. On the other hand, a very large and featureless bands is obtained in cartesian coordinates, with no detectable vibronic bands. Furthermore, due to the

large broadening, the value of the intensity maximum is significantly lower in cartesian coordinates. The spectrum has been simulated also using the simplified TD AS|FC model, in order to highlight the impact of mode-mixing effects, and the results are reported in the lower panel of figure 7. AS and AH results are nearly equivalent, which means that mode-mixing is not the main source of inaccuracies, so that the discrepancies between cartesian and internal coordinates are mainly due to an inaccurate definition of the shift vector **K**. The graphical representation of the shift vector calculated in cartesian ($\mathbf{K}_X$) and delocalized internal coordinates ($\mathbf{K}_S$), which is reported in figure 9, shows that, even if the elements of $\mathbf{K}_X$ and $\mathbf{K}_S$ associated to the low-frequency modes are similar, for the other vibrations the shift is usually larger in cartesian than in internal coordinates. As a consequence, the broadening is caused by a larger number of significantly shifted normal modes.

As mentioned above, vertical models are usually employed to recover the inaccuracy of adiabatic models in cartesian coordinates in the description of large-amplitude deformations. For 4,4'-CB, only simulations at the VG level have been performed, whereas the more refined VH model has not been used due to the presence of 5 imaginary frequencies of the excited state PES at the equilibrium geometry of the electronic ground state. The comparison of the TD VG|FC OPA spectrum with the TD AS|FC one is reported in figure 8. The VG spectrum is shifted towards higher energies with respect to the AS one since, as discussed for example in ref.15,16, the adiabatic separation energy between the PESs is different in the two models. Furthermore, even if the agreement with the internal coordinate results is improved with respect to the AH|FC results in cartesian coordinates, several discrepancies are still present. However, due to the impossibility of using the more refined VH models, it is not possible to check the impact of including the mode-mixing effects. This is a relevant limitation of vertical models with respect to the adiabatic ones in internal coordinates.

In order to check the reliability of the theoretical results, the computed OPA spectra have been compared with the experimental data (taken from ref.85) in figure 10. Since the experimental spectrum has been recorded in n-heptane solution, all the electronic structure calculations have been carried out including solvent effects by means of the PCM. Even if the low resolution of the experimental spectrum does not allow to identify single vibronic peaks, the overall bandshape is well simulated using both WICs and DICs, especially when Gaussian broadening functions with a large HWHM (400 cm^{-1}) are employed. For the sake of simplicity, the spectrum computed using cartesian coordinates has not been included in figure 10, since the results reported in figure 7 clearly show that in this case the bandshape is reproduced poorly.

In order to check the reliability of the theory presented in the previous section for emission spectroscopies, the OPE spectrum of 4,4'-CB has been computed using all the different coordinate sets at the TD AH|FC level. The results of the simulations, reported in supplemental figure S4,84 show that for the OPE spectrum as well many low-intensity transitions contribute to the spectrum in cartesian coordinates, at variance with the internal ones, resulting in a very large bandshape. The spectra collected in figure 11, show that also in this case the agreement between theoretical and experimental results85 is much better in internal coordinates than in cartesian coordinates, and the overall vibronic pattern is

reproduced satisfactory, even if slight differences in the intensity of the two main peaks are still present.

C ECD of (1S)-dehydro-epicamphore

The third system, which has been chosen to test the reliability of our theoretical formulation is (1S,4R)-4,7,7-trimethylbicyclo[2.2.1]hept-5-en-2-one (the structure is reported in figure 2), also known as (1S)-dehydro-epicamphor. From a theoretical point of view, the definition of a non-redundant set of internal coordinates for this system, as well as for other organic bicyclic compounds, is quite challenging. First of all, due to its complex topology, with two fused rings, the definition of a non-redundant Z-matrix is far from straightforward. On the other hand, DICs and WICs can be easily built since only the molecular topology is required. Even if for several years only the ECD and the CPL spectra of (1R)-camphorquinone have been measured,86 an extensive study of the experimental ECD and CPL spectra of camphore derivatives has been provided recently by Longhi and co-workers, 87 and therefore the reliability of the computational model can be checked by comparing theoretical and experimental results. Here, we will focus on (1S)-dehydro-epicamphor since, due to its flexibility upon the electronic excitation, the choice of the coordinate system is critical for a correct reproduction of the vibronic bandshape. The first bright absorption of (1S)-dehydro-epicamphor is associated to the $S_1 \leftarrow S_0$ ($\pi \rightarrow \pi^*$) electronic transition. The graphical representation of the equibrium geometries of the two electronic states, reported in figure 12, shows that the largest distorsion involves an out-of-plane motion of the carbonyl group. This deformation, as already pointed out by Longhi and co-workers,87 defines the sign of the ECD and CPL spectrum according to the so-called octant rule.88

The ECD spectra of (1S)-dehydro-epicamphore calculated at the TD AH|FC level using different coordinate systems are reported in figure S5.84 Similarly to the previous systems, DICs and WICs give nearly equivalent results, whereas the spectrum in cartesian coordinates is significantly more broadened. For the previous systems, the difference between the coordinate systems has been highlighted by analyzing the structure of the Duschinsky matrix **J**. However, as shown in figure 13, in this case little differences are visible between $\mathbf{J}_x$ and $\mathbf{J}_s$. As for imidazole, a more significant quantity to analyze is the Sharp and Rosenstock **C** matrix, which is remarkably more diagonal when internal coordinates are used, as shown in figure 13. More in detail, when internal coordinates are used, a large coupling between this vibration and the mode 47, corresponding to the $C{=}O$ stretching, is present. This large coupling arises from the inaccurate description of out-of-plane motions as linear combinations of cartesian coordinates, and it disappears if delocalized internal coordinates are used.

The theoretical results have been next compared with the spectrum recorded by Longhi and co-workers,87 shown in figure 14. It is noteworthy that, even if the resolution of the experimental spectrum is low, and single vibronic peaks cannot be detected, the reproduction of the overall bandshape is rather poor in cartesian coordinates since the convolution of all the vibronic transitions gives an excessively broadened spectrum. On the other hand, using delocalized internal coordinates, the agreement between experimental and theoretical spectra becomes satisfactory, even if a constant shift between the theoretical and the experimental

spectra is still present. Since the experimental spectrum has been recorded in ethanol solution, the optimized structures and frequencies of both electronic states have been calculated in this solvent too, using the PCM. At this level, the absolute position of the spectrum is reproduced satisfactorily, and the bandshape does not change significantly. For the sake of completeness, HT effects have been included in the simulation as well. However, unlike other camphore derivatives18, in this case the AH|FC and the AH|FCHT spectra are nearly superimposable, showing that HT effects are negligible.

V Conclusions

An algorithm to generate automatically (possibly weighted) delocalized internal coordinates, supporting also complex topologies such as fused-rings, has been designed and implemented in our general platform dedicated to the computation of vibronic structures in the electronic spectra by means of either time-dependent and time-independent approaches. As expected, for rigid systems, both cartesian and internal coordinates provide nearly equivalent results, whereas significant geometry distortions accompanying electronic transitions can be better taken into account employing internal coordinates. Indeed, off-diagonal couplings are significantly smaller in internal coordinates than in cartesian ones. Thanks to this, it is possible to define the overlap integrals as product of lower-dimensionality blocks. In this configuration, it is possible to isolate and treat adequately large-amplitude motions by including anharmonic effects for instance. Work is in progress in our laboratory along these and related directions.

In our opinion, even pending these further developments, the availability of a general and robust tool for simulating all kinds of one-photon spectra employing different sets of coordinates extends the applicability of vibronic simulations to a wider range of molecular systems, for instance of biological interest. As a result, this will lead to a further increase of the role of computational studies to complement and interpret experimental spectroscopic outcomes in terms of suitable chemical models.

Acknowledgment

The research leading to these results has received funding from the European Union's Seventh Framework Programme (FP7/2007-2013) under grant agreement No.ERC-2012-AdG-320951-DREAMS. This work was supported by Italian MIUR (FIRB 2012: Progettazione di materiali nano-eterogenei per la conversione di energia solare, protocollo: RBFR122HFZ). The high performance computer facilities of the DREAMS center (http://dreamshpc.sns.it) are acknowledged for providing computer resources.

Appendix

Starting from the Sharp and Rosenstock methodology,52 Ruhoff derived two equations to compute recursively the overlap integrals ($\langle \overline{\mathbf{v}} \mid \overline{\overline{\mathbf{v}}} \rangle$).7,54,70 In absence of temperature effects only one is of interest,

$$\langle \overline{\mathbf{0}} | \overline{\overline{\mathbf{v}}} \rangle = \frac{1}{\sqrt{2\overline{\overline{v}}_i}} \left[\mathrm{D}_i \left\langle \overline{\mathbf{0}} | \overline{\overline{\mathbf{v}}} - \overline{\overline{1}}_i \right\rangle + 2\sqrt{\overline{\overline{v}}_i - 1}\mathrm{C}_{ii} \langle \overline{\mathbf{0}} | \overline{\overline{\mathbf{v}}} - \overline{\overline{2}}_i \rangle \right] \quad (35)$$

$$+\sum_{j\neq i}\sqrt{2\bar{\bar{v}}_j}\mathrm{C}_{ij}\left\langle\bar{\mathbf{0}}|\bar{\bar{\mathbf{v}}}-\bar{\bar{\mathbf{1}}}_i-\bar{\bar{\mathbf{1}}}_j\right\rangle\Bigg] \quad (36)$$

where **C** and **D** are defined as follows:

$$\mathbf{C}=2\bar{\bar{\boldsymbol{\Gamma}}}^{1/2}\left(\mathbf{J}^T\bar{\boldsymbol{\Gamma}}\mathbf{J}+\bar{\bar{\boldsymbol{\Gamma}}}\right)^{-1}\bar{\bar{\boldsymbol{\Gamma}}}^{1/2}-\mathbf{I} \quad (37)$$

$$\mathbf{D}=\bar{\bar{\boldsymbol{\Gamma}}}^{1/2}\left(\mathbf{J}^T\bar{\boldsymbol{\Gamma}}\mathbf{J}+\bar{\bar{\boldsymbol{\Gamma}}}\right)^{-1}\mathbf{J}^T\bar{\boldsymbol{\Gamma}}\mathbf{K} \quad (38)$$

$\bar{\boldsymbol{\Gamma}}$ and $\bar{\bar{\boldsymbol{\Gamma}}}$ are diagonal matrices containing the reduced frequencies of the initial and the final state, respectively. By applying recursively equation 36, it is straightforward to show that only the overlap integral between the vibrational ground states $\langle\,\bar{\mathbf{0}}\,|\,\bar{\bar{\mathbf{0}}}\rangle$ needs to be known analytically. From there, and considering only the FC case for the sake of simplicity, one can see that vibrational progressions (overtones) will be determined from D_i and the diagonal elements of **C**, while the intensity of combination bands will depend on the off-diagonal elements C_{ij}. Thus, for combination bands to give a significant contribution to the band-shape, the elements C_{ij} must have significant magnitude. This is the reason why in chapter IV **C** has been used to visualize the mixings between the different normal modes.

References

1. Long, DA., Long, D. Raman spectroscopy. Vol. 206. McGraw-Hill New York: 1997.
2. Barron, LD. Molecular Light Scattering and Optical Activity. Cambridge University Press; 2009.
3. Macak P, Luo Y, gren H. Simulations of vibronic profiles in two-photon absorption. Chem Phys Lett. 2000; 330:447–456.
4. Scalmani G, Frisch MJ, Mennucci B, Tomasi J, Cammi R, Barone V. Geometries and properties of excited states in the gas phase and in solution: Theory and application of a time-dependent density functional theory polarizable continuum model. J Chem Phys. 2006; 124:094107.
5. Casida ME. Time-dependent density-functional theory for molecules and molecular solids. J Mol Struct. 2009; 914:3–18.
6. Barone V, Biczysko M, Bloino J, Carta L, Pedone A. Environmental and dynamical effects on the optical properties of molecular systems by time-independent and time-dependent approaches: coumarin derivatives as test cases. Comput Theor Chem. 2014; 1037:35–48.
7. Ruhoff PT. Recursion relations for multi-dimensional franck-condon overlap integrals. Chem Phys. 1994; 186:355–374.
8. Dierksen M, Grimme S. Density functional calculations of the vibronic structure of electronic absorption spectra. J Chem Phys. 2004; 120:3544–3554. [PubMed: 15268516]
9. Chang J-L. A new method to calculate franck-condon factors of multidimensional harmonic oscillators including the duschinsky effect. J Chem Phys. 2008; 128:174111. [PubMed: 18465914]
10. Mukamel S, Abe S, Islampour R. Generating function for electronic spectra of polyatomic molecules. J Phys Chem. 1985; 89:201–204. DOI: 10.1021/j100248a001
11. Tang J, Lee MT, Lin SH. Effects of the duschinsky mode-mixing mechanism on temperature dependence of electron transfer processes. J Chem Phys. 2003; 119:7188–7196.

Europe PMC Funders Author Manuscripts

12. Liang W, Ma H, Zang H, Ye C. Generalized time-dependent approaches to vibrationally resolved electronic and raman spectra: Theory and applications. International Journal of Quantum Chemistry. 2015; 115:550–563.
13. Heller EJ. The semiclassical way to molecular spectroscopy. Acc Chem Res. 1981; 14:368–375. DOI: 10.1021/ar00072a002
14. Tannor DJ, Heller EJ. Polyatomic raman scattering for general harmonic potentials. J Chem Phys. 1982; 77:202–218.
15. Barone V, Bloino J, Biczysko M, Santoro F. Fully integrated approach to compute vibrationally resolved optical spectra: From small molecules to macrosystems. J Chem Theory Comput. 2009; 5:540–554. DOI: 10.1021/ct8004744 [PubMed: 26610221]
16. Bloino J, Biczysko M, Santoro F, Barone V. General approach to compute vibrationally resolved one-photon electronic spectra. J Chem Theory Comput. 2010; 6:1256–1274. DOI: 10.1021/ct9006772
17. Baiardi A, Bloino J, Barone V. General time dependent approach to vibronic spectroscopy including franck-condon, herzberg-teller, and duschinsky effects. J Chem Theory Comput. 2013; 9:4097–4115. DOI: 10.1021/ct400450k [PubMed: 26592403]
18. Barone V, Baiardi A, Bloino J. New developments of a multifrequency virtual spectrometer: Stereo-electronic, dynamical, and environmental effects on chiroptical spectra. Chirality. 2014; 26:588–600. [PubMed: 24839096]
19. Baiardi A, Bloino J, Barone V. A general time-dependent route to resonance-raman spectroscopy including franck-condon, herzberg-teller and duschinsky effects. J Chem Phys. 2014; 141:114108. [PubMed: 25240346]
20. Egidi F, Bloino J, Cappelli C, Barone V. A robust and effective time-independent route to the calculation of resonance raman spectra of large molecules in condensed phases with the inclusion of duschinsky, herzberg-teller, anharmonic, and environmental effects. J Chem Theory Comput. 2014; 10:346–363. DOI: 10.1021/ct400932e [PubMed: 26550003]
21. Vidal LN, Egidi F, Barone V, Cappelli C. Origin invariance in vibrational resonance raman optical activity. The Journal of Chemical Physics. 2015; 142:174101. [PubMed: 25956084]
22. Banerjee S, Baiardi A, Bloino J, Barone V. Temperature dependence of radiative and non-radiative rates from time-dependent correlation function methods. Journal of Chemical Theory and Computation. 2015; doi: 10.1021/acs.jctc.5b01017
23. Nooijen M. First-principles simulation of the uv absorption spectrum of ketene. International Journal of Quantum Chemistry. 2003; 95:768–783.
24. Niu Y, Peng Q, Deng C, Gao X, Shuai Z. Theory of excited state decays and optical spectra: Application to polyatomic molecules. The Journal of Physical Chemistry A. 2010; 114:7817–7831. DOI: 10.1021/jp101568f [PubMed: 20666533]
25. Borrelli R, Peluso A. The temperature dependence of radiationless transition rates from ab initio computations. Phys Chem Chem Phys. 2011; 13:4420–4426. [PubMed: 21258672]
26. Luis JM, Bishop DM, Kirtman B. A different approach for calculating franck-condon factors including anharmonicity. The Journal of Chemical Physics. 2004; 120:813–822. [PubMed: 15267917]
27. Rodriguez-Garcia V, Yagi K, Hirao K, Iwata S, Hirata S. Franck-condon factors based on anharmonic vibrational wave functions of polyatomic molecules. The Journal of Chemical Physics. 2006; 125:014109. [PubMed: 16863289]
28. Wilson, EB. Molecular Vibrations: The Theory of Infrared and Raman Vibrational Spectra. Dover, editor. Dover Publications; Mar 1. 1980 New edition edition
29. Reimers JR. A practical method for the use of curvilinear coordinates in calculations of normal-mode-projected displacements and duschinsky rotation matrices for large molecules. J Chem Phys. 2001; 115:9103–9109.
30. Duschinsky F. ccc. Acta Physicochimica URSS. 1937; 7:551.
31. Beenken WJD, Lischka H. Spectral broadening and diffusion by torsional motion in biphenyl. J Chem Phys. 2005; 123:144311. [PubMed: 16238395]

32. Borrelli R, Peluso A. The vibrational progressions of the n-v electronic transition of ethylene: A test case for the computation of franck-condon factors of highly flexible photoexcited molecules. J Chem Phys. 2006; 125:194308. [PubMed: 17129104]
33. Borrelli R, Peluso A. The electron photodetachment spectrum of c-c_4f_8: A test case for the computation of franck-condon factors of highly flexible molecules. J Chem Phys. 2008; 128:044303. [PubMed: 18247945]
34. Cerezo J, Zuniga J, Requena A, Avila Ferrer FJ, Santoro F. Harmonic models in cartesian and internal coordinates to simulate the absorption spectra of carotenoids at finite temperatures. J Chem Theory Comput. 2013; 9:4947–4958. DOI: 10.1021/ct4005849 [PubMed: 26583413]
35. Götze JP, Karasulu B, Thiel W. Computing uv/vis spectra from the adiabatic and vertical franck-condon schemes with the use of cartesian and internal coordinates. J Chem Phys. 2013; 139:234108. [PubMed: 24359353]
36. Pedone A, Bloino J, Barone V. Role of host-guest interactions in tuning the optical properties of coumarin derivatives incorporated in mcm-41: A td-dft investigation. The Journal of Physical Chemistry C. 2012; 116:17807–17818. DOI: 10.1021/jp305294u
37. Baker J, Hehre WJ. Geometry optimization in cartesian coordinates: The end of the z-matrix? J Comput Chem. 1991; 12:606–610.
38. Fogarasi G, Zhou X, Taylor PW, Pulay P. The calculation of ab initio molecular geometries: efficient optimization by natural internal coordinates and empirical correction by offset forces. J Am Chem Soc. 1992; 114:8191–8201. DOI: 10.1021/ja00047a032
39. Pulay P, Fogarasi G. Geometry optimization in redundant internal coordinates. J Chem Phys. 1992; 96:2856–2860.
40. Peng C, Ayala PY, Schlegel HB, Frisch MJ. Using redundant internal coordinates to optimize equilibrium geometries and transition states. J Comput Chem. 1996; 17:49–56.
41. Pulay P, Fogarasi G, Pongor G, Boggs JE, Vargha A. Combination of theoretical ab initio and experimental information to obtain reliable harmonic force constants. scaled quantum mechanical (qm) force fields for glyoxal, acrolein, butadiene, formaldehyde, and ethylene. J Am Chem Soc. 1983; 105:7037–7047. DOI: 10.1021/ja00362a005
42. Pulay P, Fogarasi G, Zhou X, Taylor PW. Ab initio prediction of vibrational spectra: A database approach. Vib Spectrosc. 1990; 1:159–165.
43. Natanson GA, Garrett BC, Truong TN, Joseph T, Truhlar DG. The definition of reaction coordinates for reaction-path dynamics. J Chem Phys. 1991; 94:7875–7892.
44. Jensen F, Palmer DS. Harmonic vibrational analysis in delocalized internal coordinates. J Chem Theory Comput. 2011; 7:223–230. DOI: 10.1021/ct100463a [PubMed: 26606235]
45. Baiardi A, Bloino J, Barone V. Accurate simulation of resonance-raman spectra of flexible molecules: An internal coordinates approach. J Chem Theory Comput. 2015; 11:3267–3280. DOI: 10.1021/acs.jctc.5b00241 [PubMed: 26575763]
46. Baker J, Kessi A, Delley B. The generation and use of delocalized internal coordinates in geometry optimization. J Chem Phys. 1996; 105:192–212.
47. Barone V, Baiardi A, Biczysko M, Bloino J, Cappelli C, Lipparini F. Implementation and validation of a multi-purpose virtual spectrometer for large systems in complex environments. Phys Chem Chem Phys. 2012; 14:12404–12422. [PubMed: 22772710]
48. Eckart C. Some studies concerning rotating axes and polyattomic molecules. Phys Rev. 1935; 47:552–558.
49. Franck J. Elementary processes of photochemical reactions. Transactions of the Faraday Society. 1926; 21:536–542.
50. Condon E. Nuclear motions associated with electron transitions in diatomic molecules. Phys Rev. 1928; 32:858–872.
51. Herzberg ETG. Vibrational structure of electronic transitions for polyatomic molecules. Z Phys Chem. 1933; 21:410.
52. Sharp TE, Rosenstock HM. Franck-condon factors for polyatomic molecules. J Chem Phys. 1964; 41:3453–3463.

53. Biczysko M, Piani G, Pasquini M, Schiccheri N, Pietraperzia G, Becucci M, Pavone M, Barone V. On the properties of microsolvated molecules in the ground (s[sub 0]) and excited (s[sub 1]) states: The anisole-ammonia 1:1 complex. J Chem Phys. 2007; 127:144303. [PubMed: 17935391]
54. Santoro F, Improta R, Lami A, Bloino J, Barone V. Effective method to compute franck-condon integrals for optical spectra of large molecules in solution. J Chem Phys. 2007; 126:084509. [PubMed: 17343460]
55. Bloino J, Biczysko M, Crescenzi O, Barone V. Integrated computational approach to vibrationally resolved electronic spectra: Anisole as a test case. J Chem Phys. 2008; 128:244105. [PubMed: 18601315]
56. Torii H, Tasumi M. Vibrational structure and temperature dependence of the electronic absorption (11bu .rarw. 11ag) of all-trans-.beta.-carotene. The Journal of Physical Chemistry. 1990; 94:227–231. DOI: 10.1021/j100364a037
57. Liang KK, Mebel AM, Lin SH, Hayashi M, Selzle HL, Schlag EW, Tachiya M. Influence of distortion and duschinsky effects on marcus-type theories of electron transfer rate. Phys Chem Chem Phys. 2003; 5:4656–4665.
58. Ianconescu R, Pollak E. Photoinduced cooling of polyatomic molecules in an electronically excited state in the presence of dushinskii rotations. J Phys Chem A. 2004; 108:7778–7784. DOI: 10.1021/jp037739q
59. Baiardi A, Latouche C, Bloino J, Barone V. Accurate yet feasible computations of resonance raman spectra for metal complexes in solution: $[ru(bpy)^3]^{2+}$ as a case study. Dalton Trans. 2014; 43:17610–17614. [PubMed: 25207752]
60. Lindh R, Bernhardsson A, Schätz M. Force-constant weighted redundant coordinates in molecular geometry optimizations. Chem Phys Lett. 1999; 303:567–575.
61. Lindh R, Bernhardsson A, Karlstrom G, Malmqvist P-A. On the use of a hessian model function in molecular geometry optimizations. Chem Phys Lett. 1995; 241:423–428.
62. Swart M, Matthias Bickelhaupt F. Optimization of strong and weak coordinates. Int J Quantum Chem. 2006; 106:2536–2544.
63. Hoy A, Mills I, Strey G. Anharmonic force constant calculations. Mol Phys. 1972; 24:1265–1290. DOI: 10.1080/00268977200102361
64. Bakken V, Helgaker T. The efficient optimization of molecular geometries using redundant internal coordinates. J Chem Phys. 2002; 117:9160–9174.
65. Jackels CF, Gu Z, Truhlar DG. Reaction path potential and vibrational frequencies in terms of curvilinear internal coordinates. J Chem Phys. 1995; 102:3188–3201.
66. Page M, McIver JW. On evaluating the reaction path hamiltonian. J Chem Phys. 1988; 88:922–935.
67. Brandhorst K, Grunenberg J. Efficient computation of compliance matrices in redundant internal coordinates from cartesian hessians for nonstationary points. J Chem Phys. 2010; 132:184101.
68. Grochowski P. Rotational symmetry of the molecular potential energy in the cartesian coordinates. Theor Chem Acc. 2008; 121:257–266.
69. Miyazawa T. Symmetrization of secular determinant for normal vibration calculation. J Chem Phys. 1958; 29:246–246.
70. Biczysko, M., Bloino, J., Santoro, F., Barone, V. Time independent approaches to simulate electronic spectra lineshapes: from small molecules to macrosystems. Computational Strategies for Spectroscopy, from Small Molecules to Nano Systems. Barone, V., editor. Wiley; Chichester: 2011. p. 361-443.
71. Karasulu B, Götze JP, Thiel W. Assessment of franck-condon methods for computing vibrationally broadened uv-vis absorption spectra of flavin derivatives: Riboflavin, roseoflavin, and 5-thioflavin. J Chem Theory Comput. 2014; 10:5549–5566. DOI: 10.1021/ct500830a [PubMed: 26583238]
72. Santoro F, Lami A, Improta R, Bloino J, Barone V. Effective method for the computation of optical spectra of large molecules at finite temperature including the duschinsky and herzberg–teller effect: The q_x band of porphyrin as a case study. J Chem Phys. 2008; 128:224311. [PubMed: 18554017]
73. Frisch, MJ., Trucks, GW., Schlegel, HB., Scuseria, GE., Robb, MA., Cheeseman, JR., Scalmani, G., Barone, V., Mennucci, B., Petersson, GA., Nakatsuji, H., et al. Gaussian development version, revision i.03. gaussian, Inc; Wallingford CT: 2015.

74. Becke AD. Density-functional thermochemistry. iii. the role of exact exchange. J Chem Phys. 1993; 98:5648–5652.
75. Double and triple-ζ basis sets of sns family. are available for download. http://compchem.sns.it/downloads
76. Barone V, Cimino P. Accurate and feasible computations of structural and magnetic properties of large free radicals: The pbe0/n07d model. Chem Phys Lett. 2008; 454:139–143.
77. Barone V, Cimino P, Stendardo E. Development and validation of the b3lyp/n07d computational model for structural parameter and magnetic tensors of large free radicals. J Chem Theory Comput. 2008; 4:751–764. DOI: 10.1021/ct800034c [PubMed: 26621090]
78. Tomasi J, Mennucci B, Cammi R. Quantum mechanical continuum solvation models. Chem Rev. 2005; 105:2999–3094. DOI: 10.1021/cr9904009 [PubMed: 16092826]
79. Mennucci B. Polarizable continuum model. Wiley Interdiscip Rev: Comput Mol Sci. 2012; 2:386–404.
80. Cances E, Mennucci B, Tomasi J. A new integral equation formalism for the polarizable continuum model: Theoretical background and applications to isotropic and anisotropic dielectrics. J Chem Phys. 1997; 107:3032–3041.
81. Jarzecki AA, Spiro TG. Ab initio computation of the uv resonance raman intensity pattern of aqueous imidazole. J Raman Spectrosc. 2001; 32:599–605.
82. Jarzecki AA. Quantum-mechanical calculations of resonance raman intensities: The weighted-gradient approximation. J Phys Chem A. 2009; 113:2926–2934. DOI: 10.1021/jp8095715 [PubMed: 19260673]
83. Balakrishnan G, Jarzecki AA, Wu Q, Kozlowski PM, Wang D, Spiro TG. Mode recognition in uv resonance raman spectra of imidazole: Histidine monitoring in proteins. J Phys Chem B. 2012; 116:9387–9395. DOI: 10.1021/jp305083t [PubMed: 22779777]
84. See supplemental material at [URL will be inserted by AIP] for figures S1, S2, S3, S4, S5 .
85. Kukielski J. Molecular interactions of 4-n-alkyl-4-n'-cyanobiphenyl detected in vibronic and vibrational spectra. Journal of Molecular Structure. 1999; 478:1–8.
86. Luk CK, Richardson FS. Circularly polarized luminescence spectrum of camphorquinone. Journal of the American Chemical Society. 1974; 96:2006–2009. DOI: 10.1021/ja00814a004
87. Longhi G, Castiglioni E, Abbate S, Lebon F, Lightner DA. Experimental and calculated cpl spectra and related spectroscopic data of camphor and other simple chiral bicyclic ketones. Chirality. 2013; 25:589–599. [PubMed: 23840012]
88. Alison Rodger, BN. Circular dichroism and linear dichroism. Oxford university press; 1997.

Europe PMC Funders Author Manuscripts

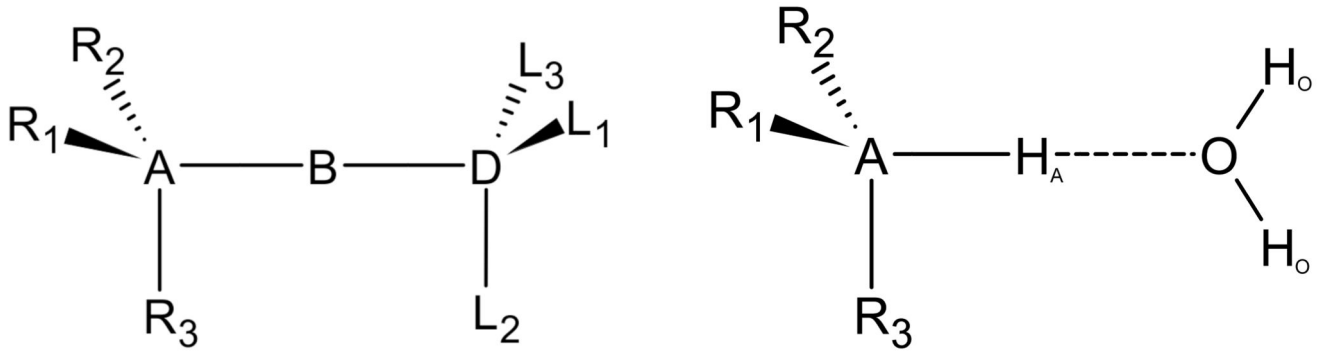

Fig. 1.

Upper panel: graphical representation of linear structures within a molecule. The three collinear atoms are labelled as *A*, *B* and *D*, and the atoms bonded to *A* and *D* are indicated as L_i and R_i, respectively, where *i* is an integer number. Lower panel: graphical representation of an hydrogen bond between the hydrogen atom bonded to the generic atom A and a water molecule. For the sake of clarity, the hydrogen bonded to A has been labelled as H_A, while the hydrogen atoms of the water have been labelled as H_O.

Europe PMC Funders Author Manuscripts

Europe PMC Funders Author Manuscripts

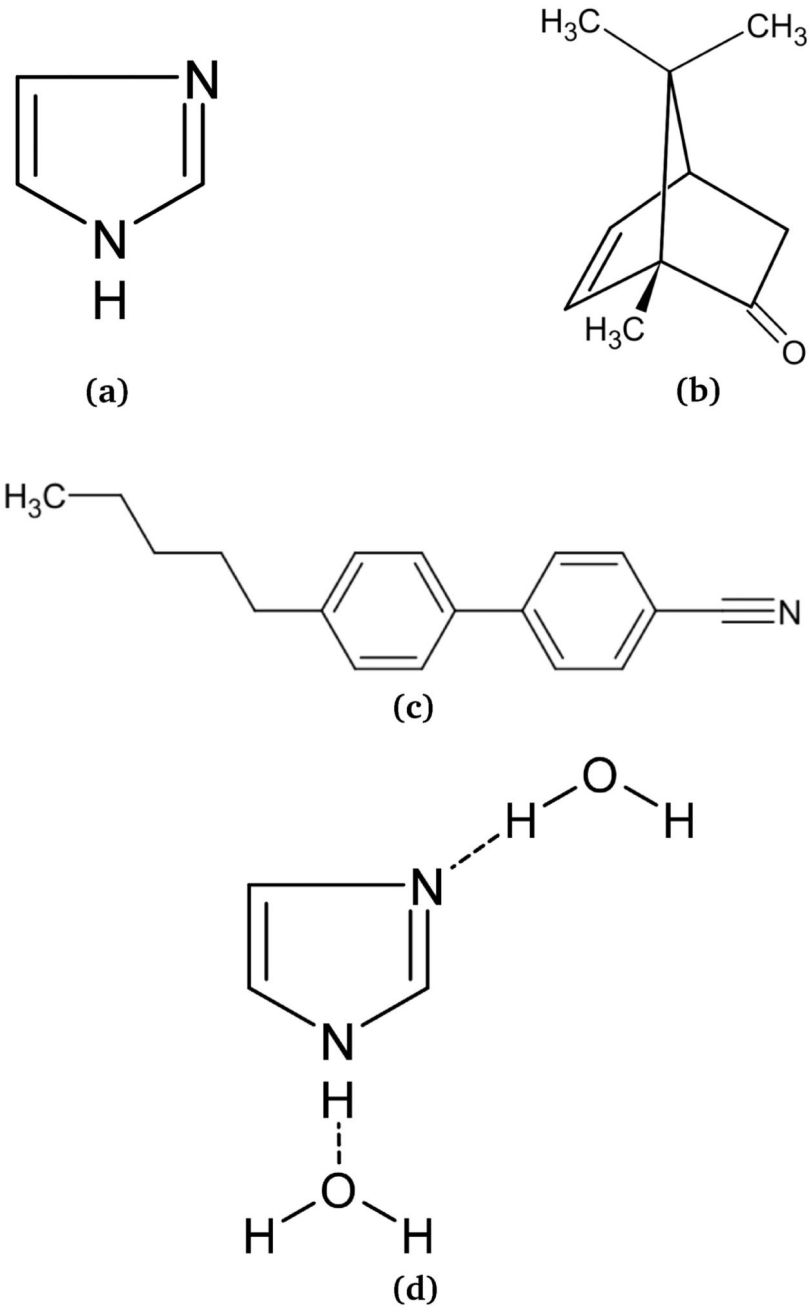

Fig. 2.

Graphical representation of the molecules studied in this work: imidazole (a), (1S)-dehydro-epicamphor (b) and 4-pentyl-4’-cyanobiphenyl (c), the complex composed by one molecule of imidazole and two molecules of water (d).

Europe PMC Funders Author Manuscripts

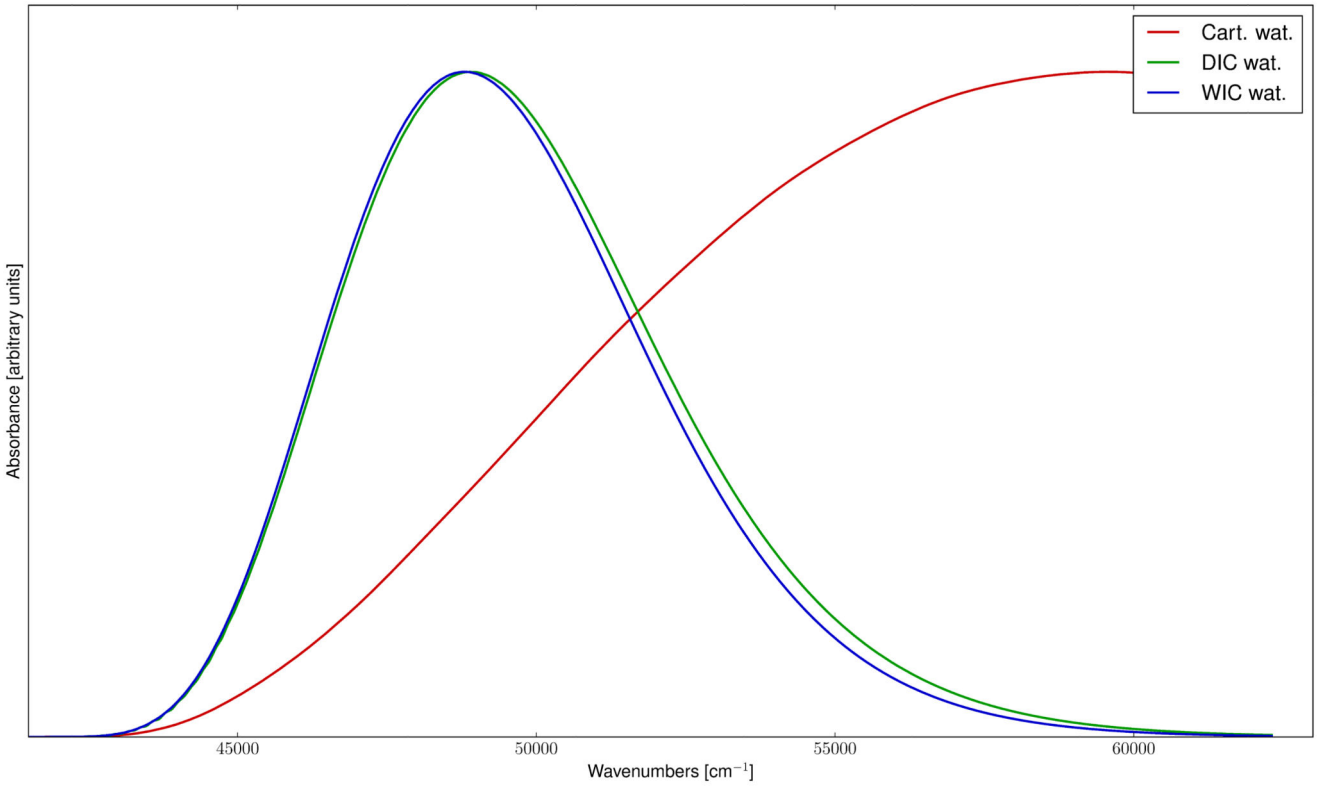

Fig. 3.

Theoretical OPA spectra of the $S_2 \leftarrow S_0$ transition of imidazole in water simulated at the TD AH|FC level using cartesian (red line) delocalized (green line) and weighted internal coordinates (blue line). Gaussian broadening functions with HWHM of 100 cm^{-1} have been used to simulate broadening effects.

Europe PMC Funders Author Manuscripts

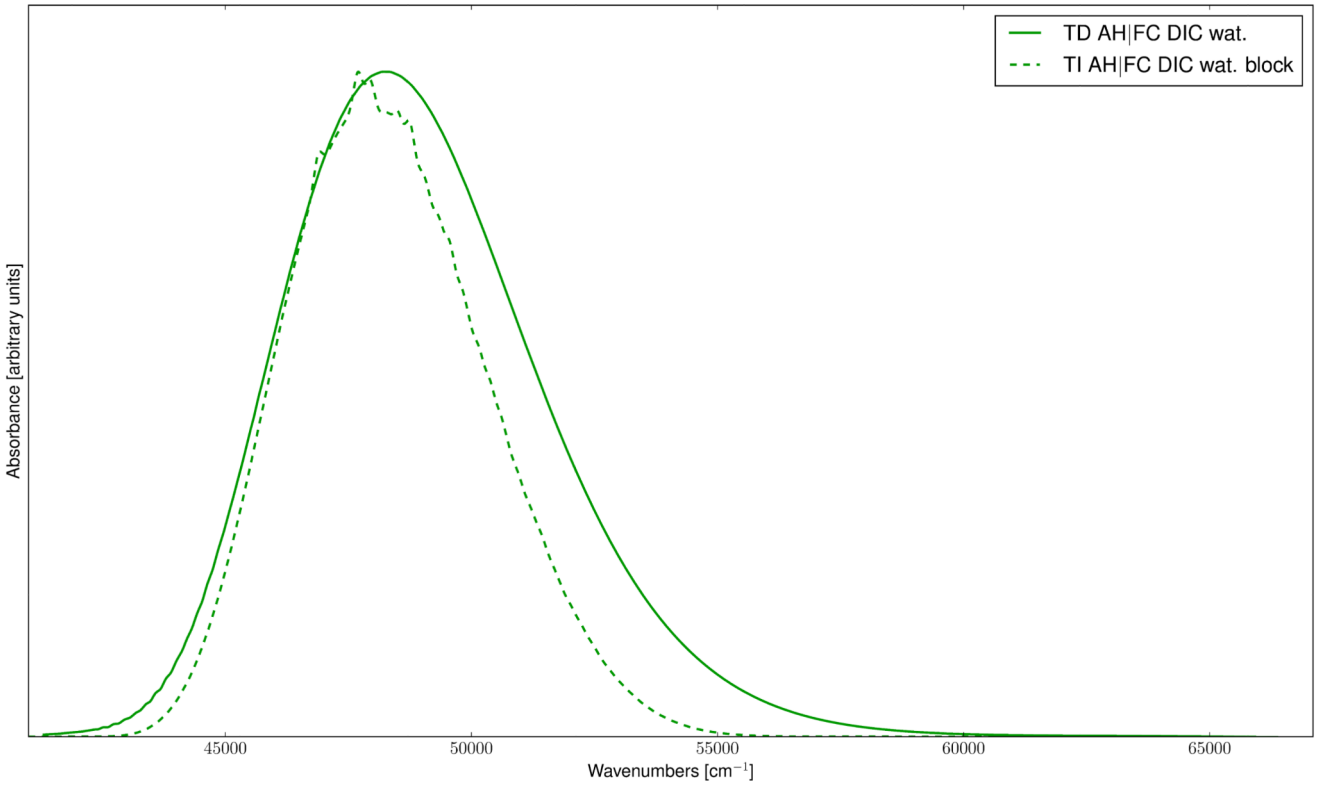

Fig. 4.

Theoretical OPA spectra of the $S_2 \leftarrow S_0$ transition of imidazole in water simulated at the TD AH|FC level using DICs with the full Duschinsky matrix (solid green line) and a block Duschinsky matrix, where the coupling elements between the five lowest energy normal modes and the other modes have been neglected. Gaussian broadening functions with HWHM of 100 cm^{-1} have been used to simulate the broadening effects.

Europe PMC Funders Author Manuscripts

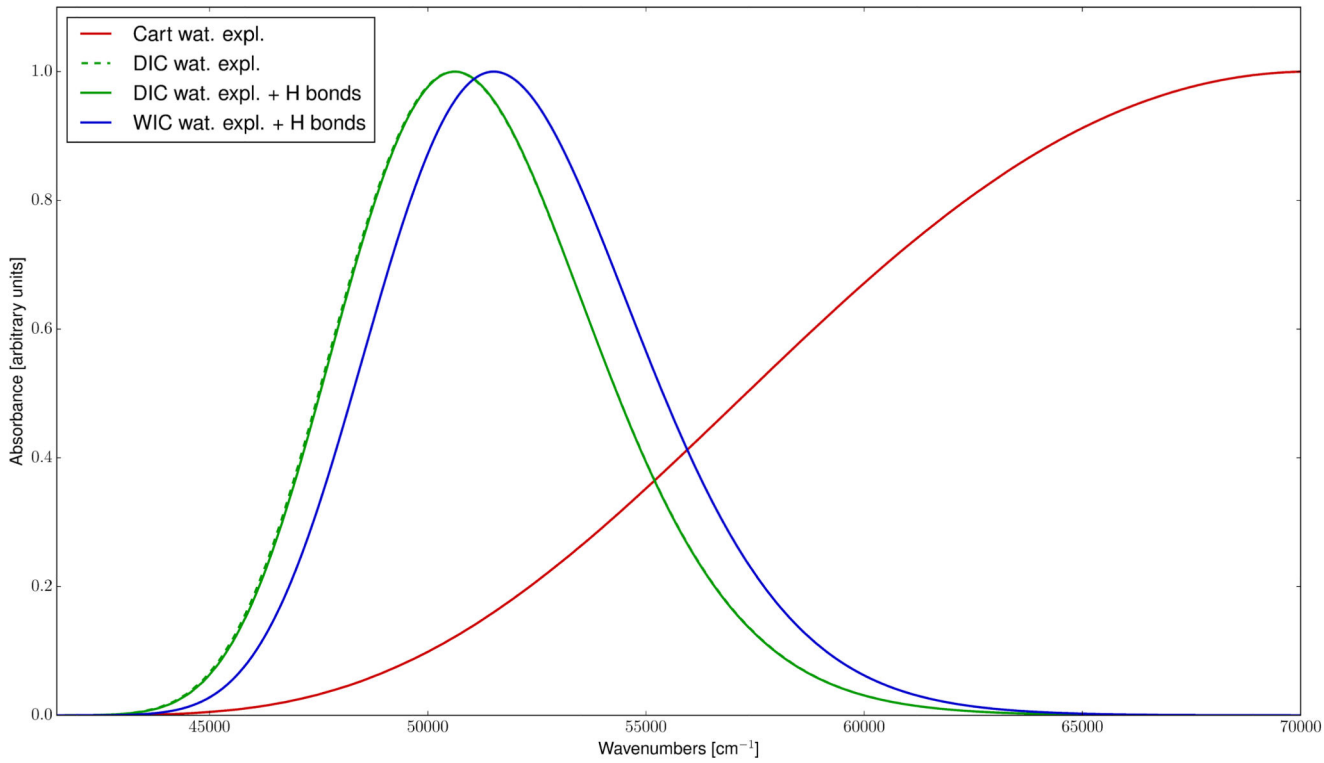

Fig. 5.

Theoretical OPA spectra of the $S_2 \leftarrow S_0$ transition of imidazole in water, where solvent effects have been simulated adding two explicit water molecules in the QM calculation. All simulations have been performed at the TD AH|FC level, using cartesian (red line), delocalized (green line) and weighted internal coordinates (blue line) using the standard connectivity matrix (solid lines) and the one, which has been modified to support the presence of hydrogen bonds (dashed lines). Gaussian distribution functions with HWHM of 100 cm^{-1} have been used to reproduce broadening effects.

Europe PMC Funders Author Manuscripts

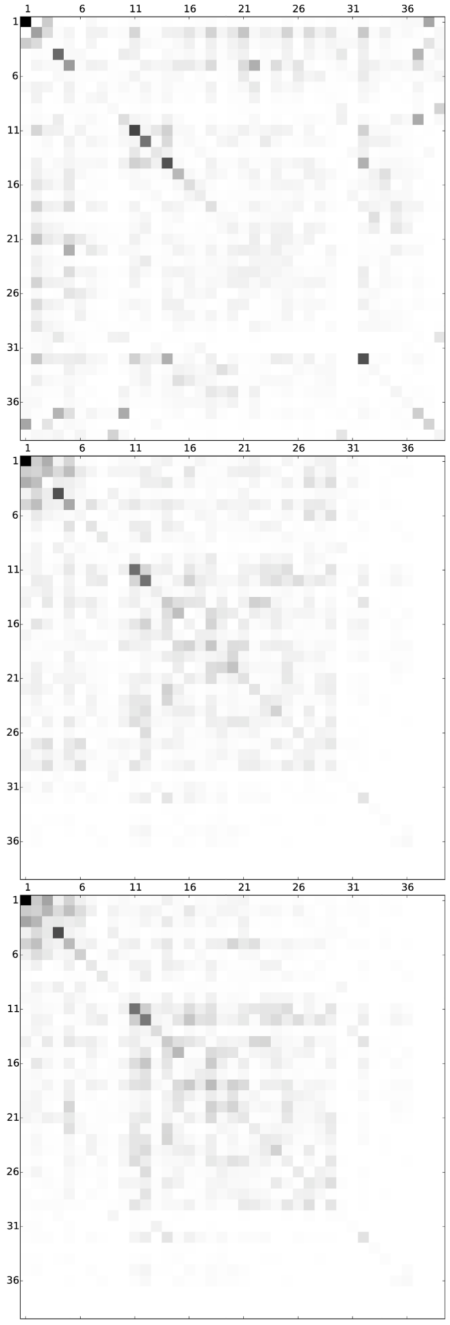

Fig. 6.

Graphical representation of the Sharp and Rosenstock matrix **C** for the $S_2 \leftarrow S_0$ transition of imidazole in water at the VH|FC level. Solvent effects have been included by performing the calculations on the cluster, shown in figure 2. The representation is obtained by calculating the square of the elements of **C** and normalizing them with respect to the maximum value of C_{ij}^2 (0.51 for Cart., 0.32 for DICs in both cases). In order to facilitate the visual comparison, the highest maximum (0.51) was used to divide each element of the three

matrices. A shade of gray is associated to each element (*i,j*) in the figure with white for 0 and black for 1.

Europe PMC Funders Author Manuscripts

Europe PMC Funders Author Manuscripts

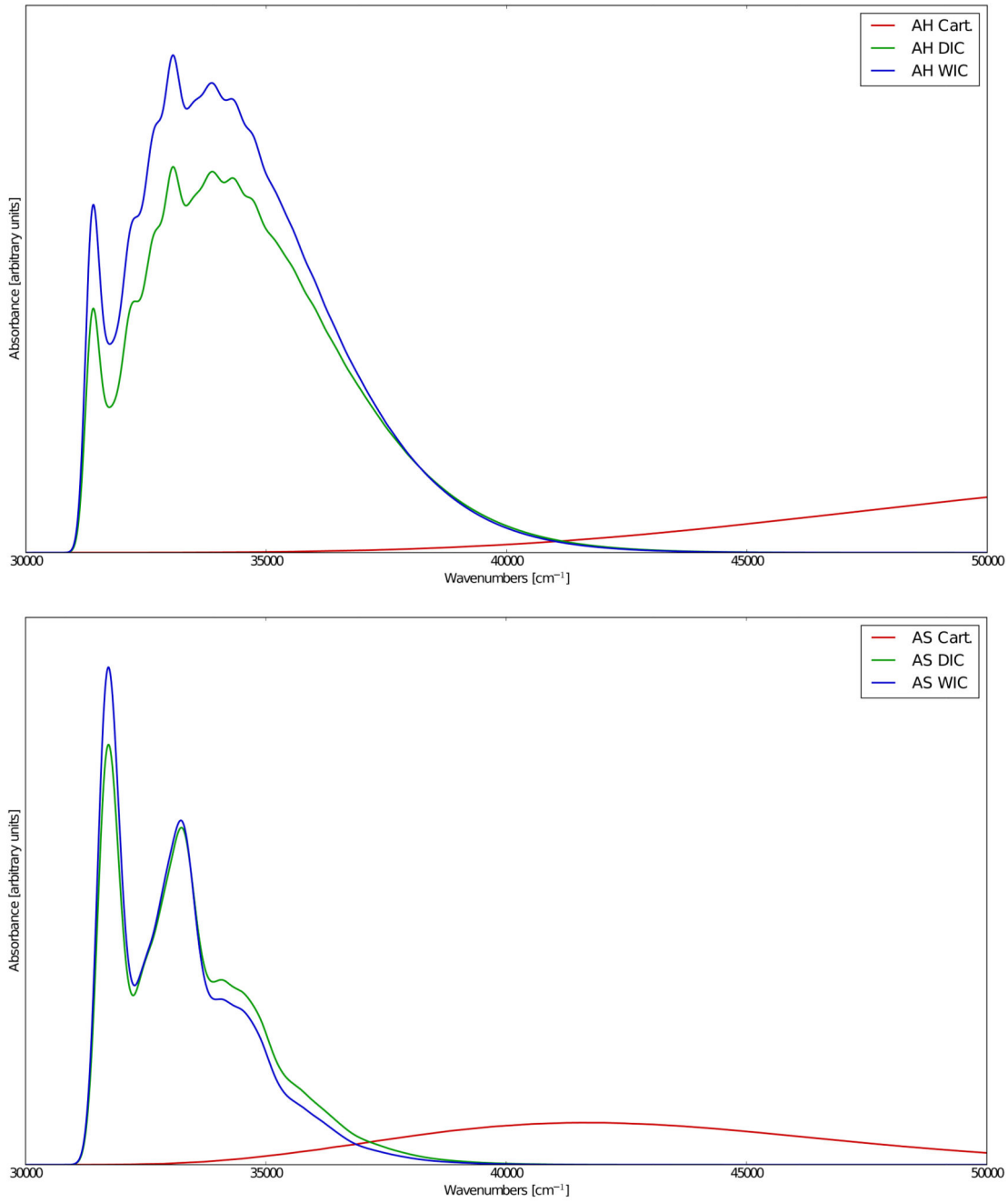

Fig. 7.

Theoretical OPA spectrum for the $S_1 \leftarrow S_0$ transition of 4,4'-CB calculated in vacuum at the TD AH|FC (upper panel) and TD AS|FC (lower panel) levels using cartesian coordinates (solid red line), DICs (solid green line) and WICs (solid blue line). Gaussian distribution functions with HWHM of 100 cm^{-1} have been used to reproduce broadening effects.

Europe PMC Funders Author Manuscripts

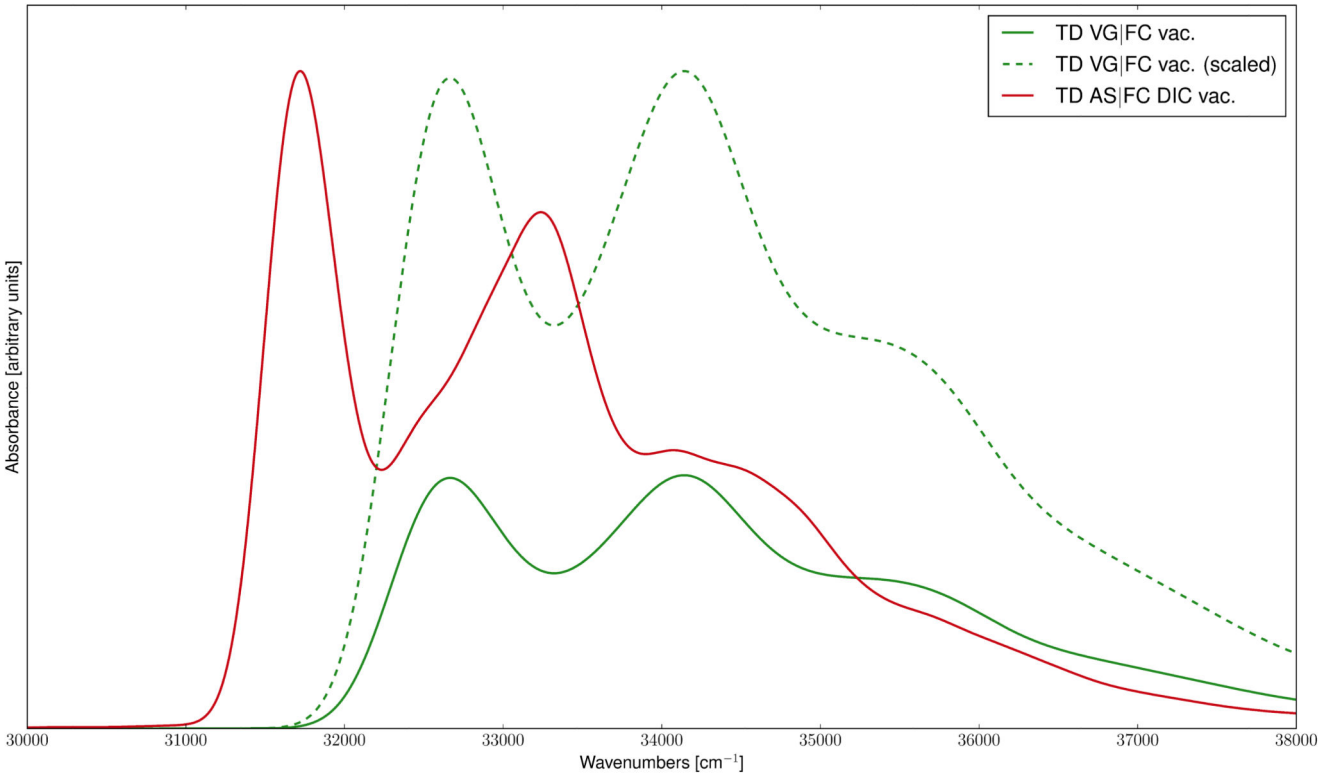

Fig. 8.

Theoretical OPA spectrum for the $S_1 \leftarrow S_0$ transition of 4,4'-CB calculated at the TD AS|FC (solid red line) with DICs, and at the TD VG|FC (solid green line) level. The TD VG|FC spectrum, scaled by a factor of 2.59 to match the intensity of the maximum with the one of the TD AS|FC spectrum, is also reported (dashed green line). Gaussian distribution functions with HWHM of 100 cm^{-1} have been used to reproduce broadening effects.

Europe PMC Funders Author Manuscripts

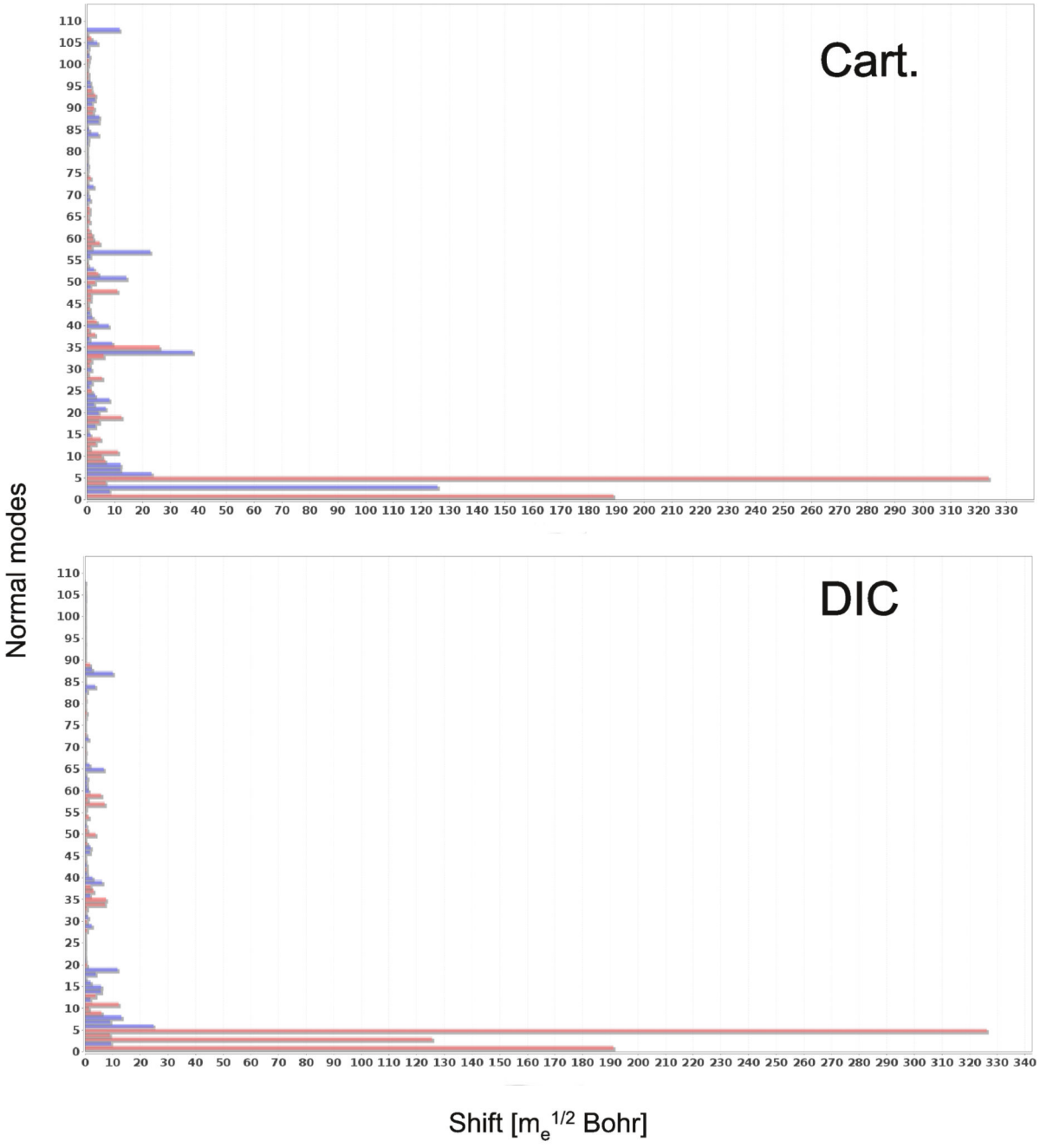

Fig. 9.

Graphical representation of the shift vector **K** relative to the $S_1 \leftarrow S_0$ transition of 4,4'-CB in cartesian (upper panel) and delocalized internal coordinates (lower panel). Positive shifts are indicated with red bars, while the negative ones with blue bars.

Europe PMC Funders Author Manuscripts

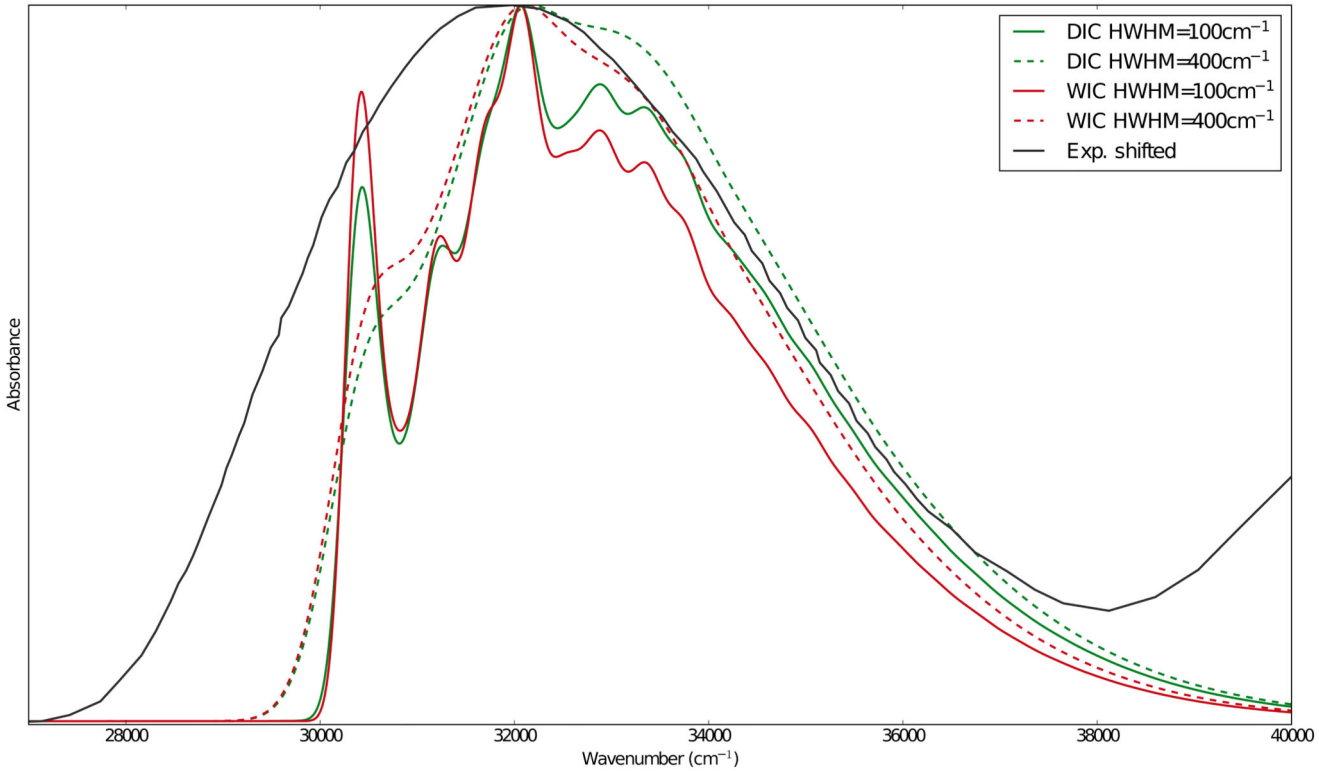

Fig. 10.

Theoretical OPA spectrum for the $S_1 \leftarrow S_0$ transition of 4,4'-CB calculated in n-heptane at the TD AH|FC level using delocalized (solid green line) and weighted internal coordinates (solid blue line), together with the experimental spectrum, taken from ref.85 Solvent effects have been included by means of PCM. Gaussian distribution functions with HWHM of 100 cm^{-1} have been used to reproduce broadening effects.

Europe PMC Funders Author Manuscripts

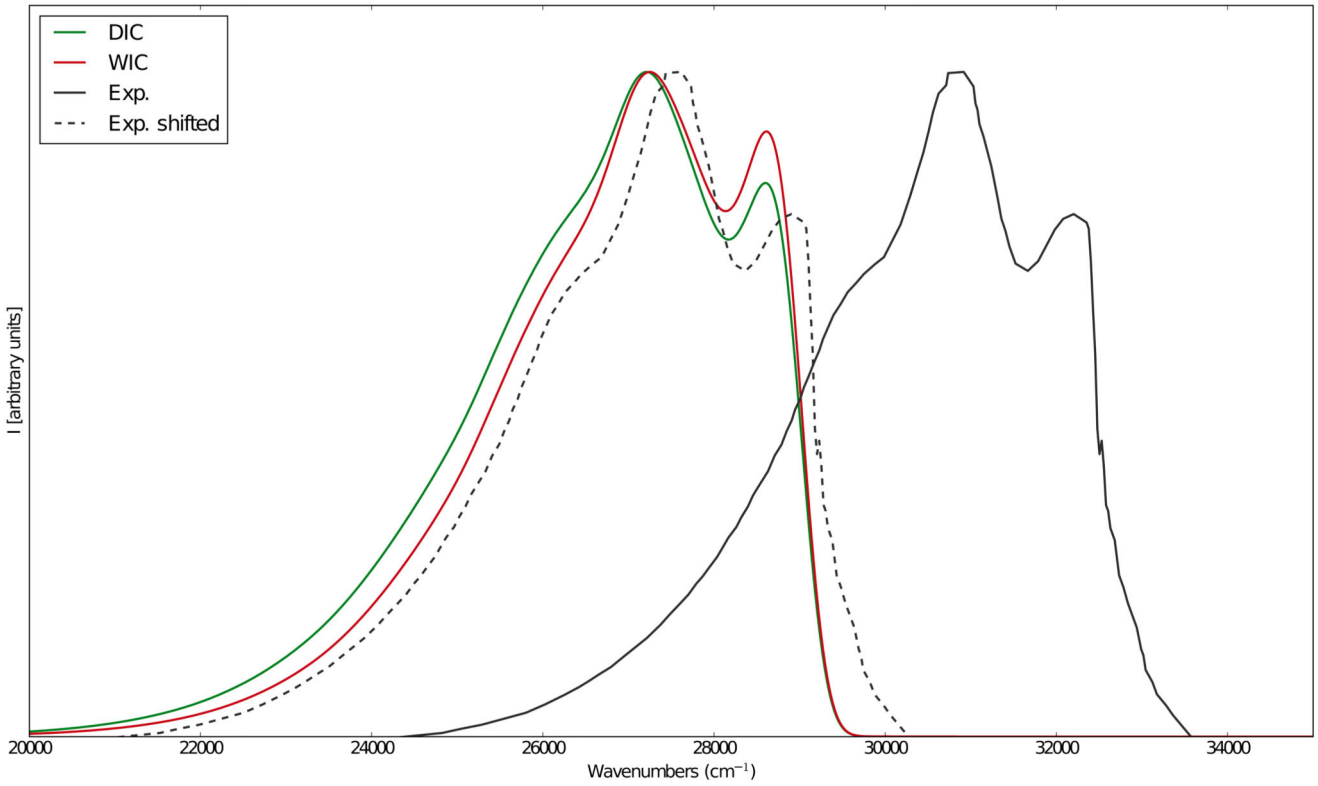

Fig. 11.

Comparison between the theoretical OPE spectra for the $S_1 \rightarrow S_0$ transition of 4,4'-CB calculated in n-heptane at the TD AH|FC level using delocalized internal coordinates (green line) and weighted internal coordinates (red line). Gaussian distribution functions with HWHM of 100 cm^{-1} (solid lines) and 400 cm^{-1} (dashed lines) have been used to reproduce broadening effects. The experimental spectrum is also reported (dashed, black lines, taken from ref.85), to which a constant shift of 4500 cm^{-1} has been applied, in order to facilitate the comparison with the theoretical results.

Europe PMC Funders Author Manuscripts

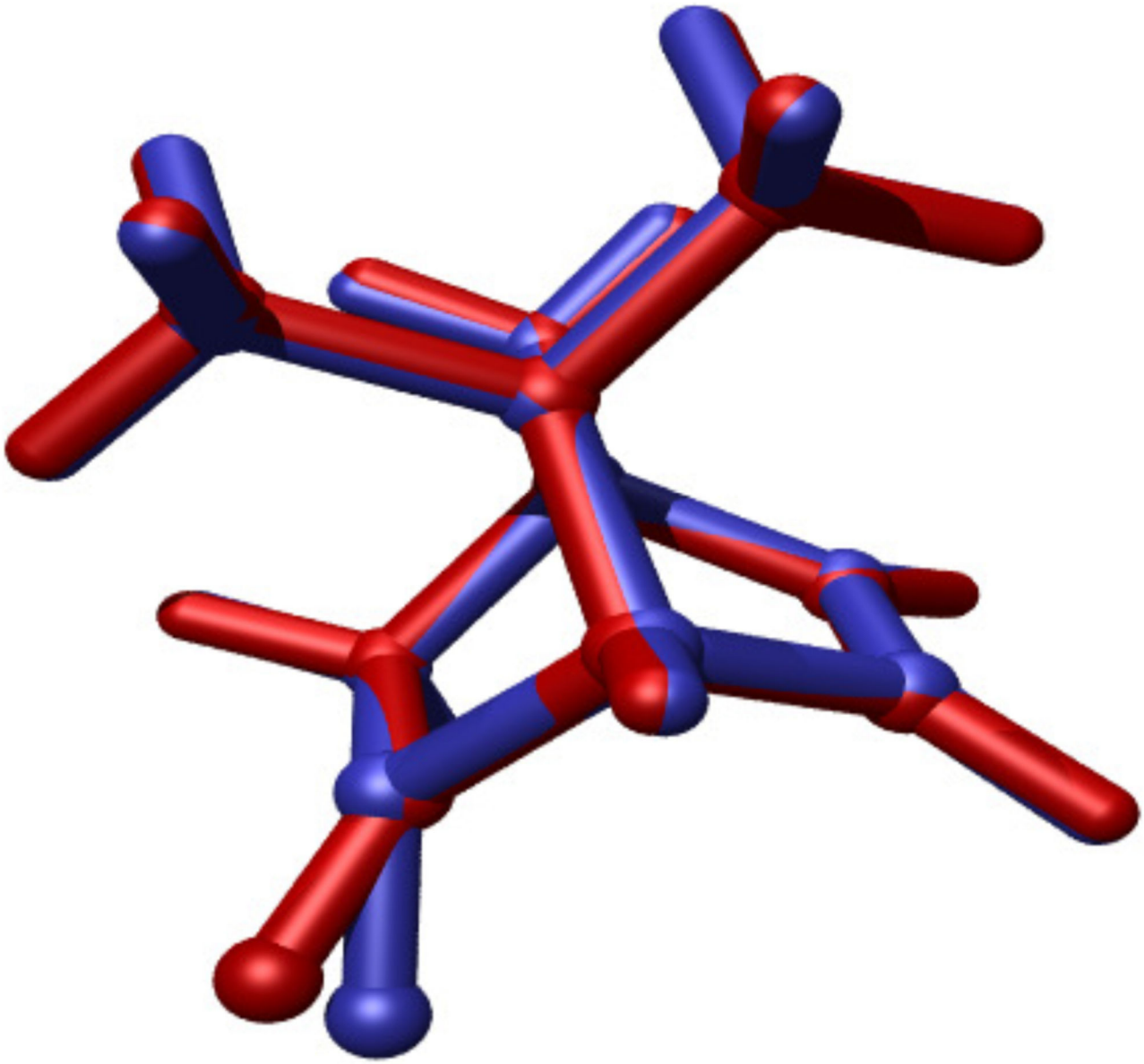

Fig. 12.

Graphical representation of the optimized structures of the S_0 (red) and S_1 (blue) electronic states of (1S)-dehydro-epicamphor

Europe PMC Funders Author Manuscripts

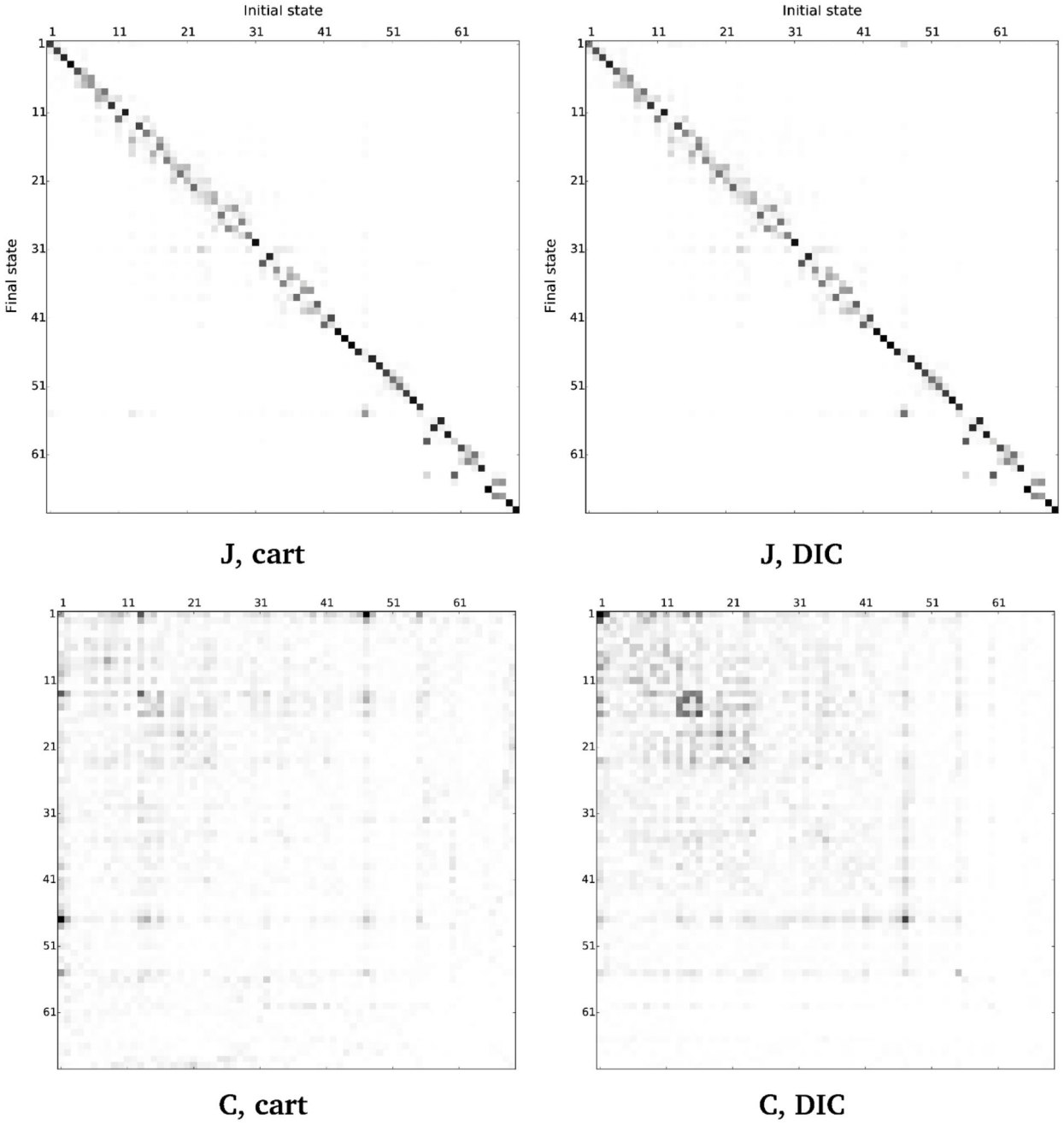

Fig. 13.

Graphical representation of the Duschinsky matrix **J** (upper panels) and of the Sharp and Rosenstock matrix **C** (lower panels) for the $S_1 \leftarrow S_0$ transition of (1S)-dehydro-epicamphor in vacuum using cartesian (left panels) and delocalized internal coordinates (right panels). The representation of the Duschinsky matrix is obtained as follows: the elements $J_{ij}^2 / \left(\sum_{i=1}^{N} J_{ij}^2 \right)$ are calculated and a shade of gray is associated to each element (i,j) in the

figure based on the equivalence (0, white; 1, black). The representation of **C** is obtained as in figure 6 for **C**.

Europe PMC Funders Author Manuscripts

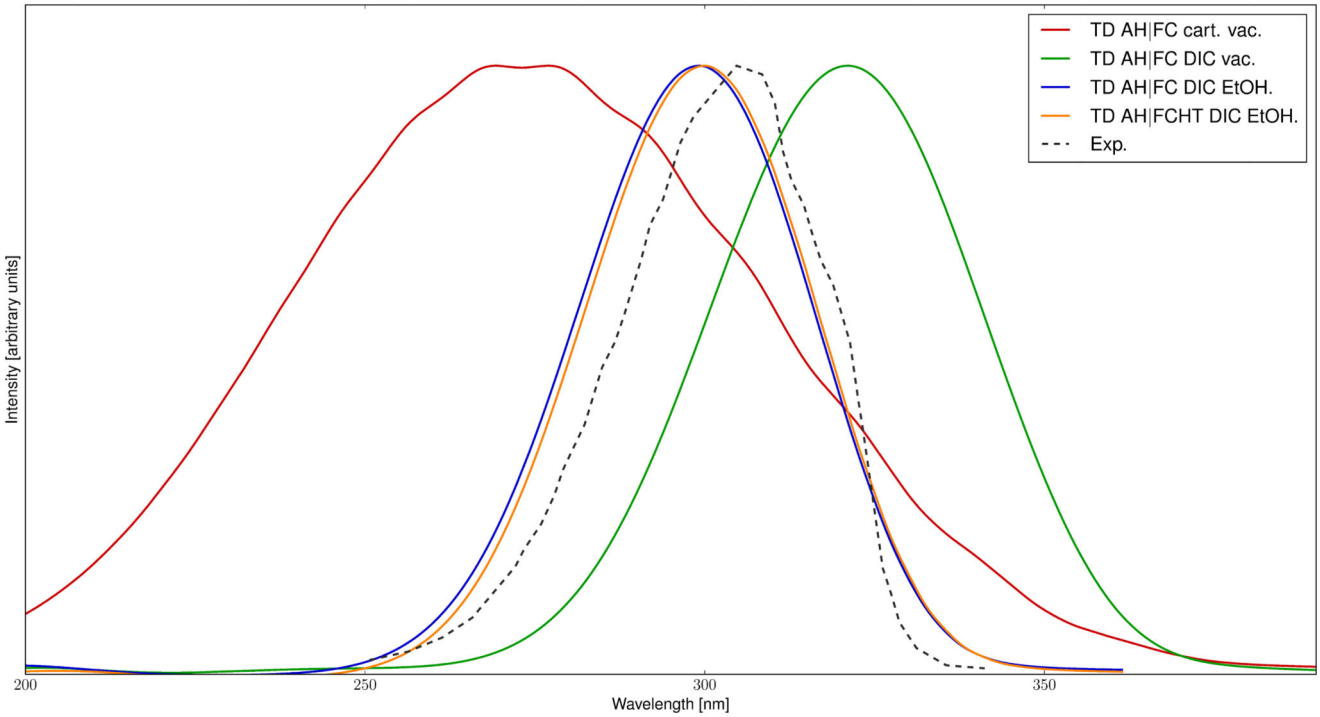

Fig. 14.

Comparison between the experimental ECD spectrum for the $S_1 \leftarrow S_0$ transition of (1S)-dehydroepicamphor (taken from ref.87) and the theoretical results in cartesian and delocalized internal coordinates computed at the TD AH|FC levels in vacuum and solvent (ethanol). Solvent effects have been included by means of PCM. Gaussian distribution functions with HWHM of 100 cm^{-1} have been used to reproduce broadening effects.

Europe PMC Funders Author Manuscripts

Table I

Equivalence table giving the quantities, to use in equation 1 for the different types of one-photon spectroscopies.

OPA:	$I = \varepsilon(\omega)$	$\alpha = \frac{10\pi\mathcal{N}_A}{3\,\epsilon_0 \ln(10)\hbar c}$	$\beta = 1 \;\; \gamma = m \;\; \boldsymbol{d}^{\mathrm{A}}_{mn} = \boldsymbol{d}^{\mathrm{B}}_{mn} = \boldsymbol{\mu}_{mn}$
OPE:	$I = I_{em}/N_n$	$\alpha = \frac{2\mathcal{N}_A}{3\,\epsilon_0 c^3}$	$\beta = 4 \;\; \gamma = n \;\; \boldsymbol{d}^{\mathrm{A}}_{mn} = \boldsymbol{d}^{\mathrm{B}}_{mn} = \boldsymbol{\mu}_{mn}$
ECD:	$I = \Delta\varepsilon(\omega)$	$\alpha = \frac{40\mathcal{N}_A\pi}{3\,\epsilon_0 \ln(10)\hbar c^2}$	$\beta = 1 \;\; \gamma = m \;\; \boldsymbol{d}^{\mathrm{A}}_{mn} = \boldsymbol{\mu}_{mn}\,, \;\; \boldsymbol{d}^{\mathrm{B}}_{mn} = \mathfrak{I}(\boldsymbol{m}_{mn})$
CPL:	$I = \Delta I_{em}/N_n$	$\alpha = \frac{8\mathcal{N}_A}{3\,\epsilon_0 c^4}$	$\beta = 4 \;\; \gamma = n \;\; \boldsymbol{d}^{\mathrm{A}}_{mn} = \boldsymbol{\mu}_{mn}\,, \;\; \boldsymbol{d}^{\mathrm{B}}_{mn} = \mathfrak{I}(\boldsymbol{m}_{mn})$